



On the Distortional-Global Interaction in Cold-Formed Steel Columns: Relevance, Post-Buckling Behavior, Strength and DSM Design

André Dias Martins¹, Dinar Camotim¹, Pedro Borges Dinis¹

Abstract

This work reports the available results of an ongoing numerical (shell finite element) investigation on the post-buckling behavior, strength and design of fixed-ended cold-formed steel columns undergoing distortional-global (D-G) interaction. Column with different cross-section shapes are analyzed, namely plain lipped channel (LC), web-stiffened lipped channel (WSLC) and zed-section (Z) columns, in order to investigate distinct D-G interaction natures: involving either distortional and (global) flexural-torsional buckling (LC and WSLC columns) or distortional and (global) minor-axis flexural buckling (Z columns). In particular, the relevance of these D-G interaction types is discussed, by assessing when they affect visibly the column ultimate strength and/or failure mode. The results presented and discussed concern columns with various geometries and yield stresses, thus ensuring a wide variety of range combinations involving (i) global-to-distortional critical buckling load ratios (R_{GD}) and (ii) squash-to-non critical buckling (distortional or global) load ratios (R_y) and leading to non-negligible failure load erosion. The possible occurrence and failure load impact of “secondary (distortional or global)-bifurcation D-G interaction” ($R_{GD} < 1.0$ or $R_{GD} > 1.0$ and high R_y) are investigated – it is well known that such impact may be significant in columns experiencing “true D-G interaction” ($R_{GD} \approx 1.0$). The above results consist of (i) relevant non-linear (elastic and elastic-plastic) equilibrium paths, (ii) deformed configuration evolutions along those paths, evidencing D-G interactive effects, and (iii) figures providing the failure mode characterization. Then, the numerical failure load data obtained are compared with their predictions by (i) the currently codified DSM (Direct Strength Method) column global and distortional strength curves, and (when necessary) (ii) proposed DSM-based design approaches, specifically developed to handle D-G interactive failures – a few design considerations are drawn from these comparisons.

1. Introduction

The complex shape and high wall slenderness exhibited by the open thin-walled cross-sections commonly used in cold-formed steel (CFS) members make them highly susceptible to several instability phenomena, involving either individual (local, distortional, global – L, D, G) and/or coupled (L-D, L-G, D-G, L-D-G) buckling modes. In fact, the efficient design of such elements is far from well established, since interactive buckling phenomena may emerge even when the corresponding critical buckling loads/moments are significantly apart. Therefore, in order to assess the structural behavior of such members it does not

¹ CERIS, ICIST, DECivil, Instituto Superior Técnico, Universidade de Lisboa, Portugal. <andrerdmartins@ist.utl.pt>, <dcamotim@civil.ist.utl.pt> and <dinis@civil.ist.utl.pt>

suffice to acquire in-depth knowledge on their “pure”/individual buckling and post-buckling behavior, since couplings involving two (or even three) buckling modes may occur. Naturally, such coupling effects may erode, to a smaller or larger extent, the member ultimate strength (depending on the corresponding slenderness), thus leading to a high likelihood of reaching unsafe designs.

As far as interaction phenomena involving distortional buckling in CFS columns are concerned (*e.g.*, Camotim *et al.* 2016a), most of the existing studies, comprising experimental investigations, numerical simulations and/or design proposals, deal with L-D interaction. It is worth mentioning the works of Kwon & Hancock (1992), Young *et al.* (2013) and Martins *et al.* (2015, 2016a, 2016b). However, the amount of research available on columns undergoing D-G interaction is much scarcer and, therefore, a significant research effort is needed before safe and accurate design rules against this type of interactive failure can be established/developed. Indeed, to the authors’ best knowledge, the available works addressing the influence of this coupling phenomenon on the post-buckling behavior and ultimate strength of CFS columns consist of (i) experimental investigations on rack-section uprights, with and without holes (Crisan *et al.* 2012a, Dubina *et al.* 2013), lipped channel columns (Santos *et al.* 2012)² and, more recently, web-stiffened lipped channel columns (Anbarasu & Murugapandian 2016)³, and (ii) the numerical (ii₁) shell finite element investigations on simply supported (locally/globally pinned end cross-sections with free or prevented warping) and fixed-ended lipped channel columns (Dinis & Camotim 2011a, Camotim & Dinis 2013), and simply supported and warping-prevented rack-section uprights with or without holes (Crisan *et al.* 2012b), and (ii₂) Generalized Beam Theory (GBT) study on the mechanics of fixed-ended lipped channel columns affected by this type of interaction (Martins *et al.* 2016c).

Although all the above studies provided clear evidence of the detrimental influence of D-G interaction on the column strength, an investigation concerning the relevance and DSM (Direct Strength Method) design is still lacking – this work aims at contributing towards filling this gap. Therefore, the aim of this work is to report the available results of an ongoing numerical (shell finite element) investigation on the post-buckling behavior, strength and design of fixed-ended CFS columns undergoing different levels of D-G interaction types and natures⁴ – two different D-G interaction natures are considered, differing in the nature of the global buckling mode involved: major-axis flexural-torsional (investigated with LC and WSLC columns) and minor-axis flexural (investigated with Z columns). In particular, the relevance of D-G interaction is discussed, in order to assess when the column ultimate strength and/or failure mode are visibly affected by its development. It is necessary to identify ranges of (i) global-to-distortional critical buckling load ratios (R_{GD}) and (ii) squash-to-non critical buckling (distortional or global) load ratios (R_y) leading to non-negligible ultimate strength erosion. Both columns experiencing “true D-G interaction” ($R_{GD} \approx 1.0$) and “secondary (distortional or global)-bifurcation D-G interaction” ($R_{GD} < 1.0$ or $R_{GD} > 1.0$ with high R_y values) are investigated – particular attention is paid to the former, since the impact on the ultimate strength is more significant. The results presented consist of (i) relevant non-linear equilibrium paths, (ii) deformed configuration evolutions along those paths, evidencing D-G interactive effects, and (iii) figures providing the failure mode characterization. Then, the numerical failure load data obtained are compared with their predictions by (i) the currently codified DSM column global and distortional strength curves, and (ii) proposed DSM-based design approaches, specifically developed to handle D-G interactive failures – design considerations are drawn from this comparison.

² The aim of this work was to investigate L-D-G interaction in fixed-ended lipped channel columns. However, it was later concluded that full fixity of the specimen end cross-sections had not been achieved, leading to column failures in D-G interactive modes.

³ It is still worth noting the tests reported by Rossi *et al.* (2010a,b) on cold-formed stainless steel lipped channel columns.

⁴ The nature of D-G interaction is related to the nature of the global buckling mode and the type of D-G interaction concerns the “true D-G interaction” and “secondary (distortional or global) D-G interaction” discussed below.

2. Buckling Analysis – Column Geometry Selection

The identification/selection of CFS ($E=210\text{GPa}$, $\nu=0.30$) column geometries (cross-section dimensions and lengths) prone to D-G interaction can be obtained only on the sole basis of the elastic critical buckling loads, *i.e.*, by performing “only” buckling analysis. Since it is well known that global buckling may have different natures (depending on the cross-section shape), involving either (i) flexure (usually minor-axis), (ii) torsion or (iii) flexure (usually major-axis) and torsion, the corresponding D-G interaction also exhibit different natures – the same applies to L-D-G interaction (*e.g.*, Dinis & Camotim 2016). Therefore, three cross-section shapes, namely (i) lipped channels (LC), (ii) web-stiffened lipped channels (WSLC) and zed-section (Z) columns are considered in this work – the first two “expected”⁵ to undergo interaction between distortional and (major-axis) flexural-torsional buckling, and the last one undergoing interaction between distortional and minor-axis flexural buckling. As done in similar studies, such geometries were selected through GBT buckling analysis sequences in the user-friendly code GBTUL (Bebiano *et al.* 2008).

The output of this selection procedure are 41 columns exhibiting R_{GD} values in the range $0.0 < R_{GD} \leq 2.0$ with the critical local buckling loads (P_{crL}) higher than the global and distortional ones ($P_{crL}/P_{cr.Max} > 1.0$, with $P_{cr.Max} = \max\{P_{crD}; P_{crG}\}$), thus ensuring that no interaction with local buckling occurs (*i.e.*, precluding L-D-G interaction)⁶ – they are labelled X1 to X41, where “X” may be either “LC”, “WSLC” or “Z”, and can be found in Tables 1 to 3, respectively (all WSLC columns contain “v-shaped” intermediate stiffeners formed by two walls with 45° inclination and width equal to $10\sqrt{2}$ mm). In order to study the effect of strong D-G interaction and the possible occurrence of “secondary (global or distortional) bifurcation D-G interaction”, 20 columns were selected in the $0.90 < R_{GD} < 1.10$ range and 19 columns are obtained by varying this ratio in 0.10/0.05 steps until 2.00 and 0.50. The remaining two columns were chosen to assess the merits of the currently codified global DSM curve in estimating the failure loads of columns collapsing in pure global modes (addressed in Section 4.1) and, therefore, are characterized by very low R_{GD} values – a similar study concerning the accuracy of currently codified distortional DSM curve is omitted since it was recently reported by Landesmann & Camotim (2013).

For illustrative purposes and in order to clarify the nature of the global buckling modes of columns prone to D-G interaction, Figs. 1(a₁)-(a₃) show the variation, with the length L (logarithmic scale), of the critical buckling load P_{cr} for columns with the three cross-section shapes and $R_{GD} \cong 1.0$ (columns LC3, WSLC3 and Z12 columns, respectively). Also displayed in Figs. 1(a₁)-(a₃) are the GBT modal participation diagrams, providing the contribution of the each deformation mode to the column critical buckling modes. On the other hand, Figs. 1(b₁)-(b₃) show the critical global and distortional buckling mode shapes of the three columns considered. The observation of these buckling results prompts the following remarks:

- (i) The GBT modal participations depicted in Fig. 1(a₁)-(a₂) (LC and WSLC columns) show that the P_{cr} vs. L descending branch corresponds to two distinct buckling behaviors⁷. The first involves contributions from deformation modes **2+4+6**, *i.e.*, the column buckles in a combination of major-axis flexure (**2**), torsion (**4**) and anti-symmetric distortion (**6**) (FTD)⁸ if $155 < L < 250\text{cm}$ (LC columns) or $155 < L < 300\text{cm}$ (WSLC columns). In view of the presence of mode **6**, the designation “global” is no longer strictly correct – however, for the sake of simplicity it will continue to be used in this work

⁵ As will be shown in Section 3.1, surprising behavioural features involving other (“not expected”) D-G coupling phenomena are also possible for specific shapes (configurations) of the initial geometrical imperfections.

⁶ Although it is very difficult (practically impossible) to fulfil this constraint without considering intermediate stiffeners for the most slender columns (see Section 3.2.1).

⁷ Similar conclusions were reported by Dinis & Camotim (2011a) and Camotim & Dinis (2013), for lipped channel columns.

⁸ This behavior is shared by all columns with singly symmetric cross-sections (with respect to the major-axis).

Table 1: Selected Z column geometries, buckling loads and relevant load ratios (dimensions in mm and loads in kN)

	b_w	b_f	b_l	t	$\frac{b_w}{b_f}$	$\frac{b_f}{b_l}$	L	P_{crG}	P_{crD}	R_{GD}	P_{crL}	$\frac{P_{crL}}{P_{cr,Max}}$	$\frac{P_{crL}}{P_{y,Max}}$
Z1	100	90	15.0	5.00	1.11	6.0	6000	155	1202	0.13	4002	3.33	2.11
Z2	120	100	10.0	4.67	1.20	10.0	7500	127	710	0.18	2786	3.92	1.78
Z3	150	130	10.0	4.50	1.15	13.0	5500	454	485	0.94	1793	3.70	0.32
Z4	150	130	13.0	4.50	1.15	10.0	5000	565	575	0.98	1793	3.12	0.26
Z5	160	130	13.0	4.50	1.23	10.0	5000	615	576	1.07	1654	2.69	0.23
Z6	140	140	13.0	3.55	1.00	10.8	6250	286	301	0.95	915	3.04	0.26
Z7	140	160	15.0	4.10	0.88	10.7	6250	395	407	0.97	1273	3.13	0.26
Z8	150	150	15.0	4.00	1.00	10.0	6200	405	414	0.98	1217	2.94	0.25
Z9	170	150	15.0	4.50	1.13	10.0	6000	584	545	1.07	1573	2.69	0.24
Z10	180	150	15.0	5.00	1.20	10.0	6250	654	699	0.94	2047	2.93	0.26
Z11	120	120	10.0	3.00	1.00	12.0	5500	194	196	0.99	654	3.33	0.27
Z12	120	100	10.0	4.50	1.20	10.0	3250	639	648	0.99	2198	3.39	0.28
Z13	100	100	10.0	3.50	1.00	10.0	3500	329	349	0.94	1234	3.54	0.31
Z14	100	90	10.0	3.50	1.11	9.0	3000	387	393	0.98	1254	3.19	0.26
Z15	130	130	10.0	3.00	1.00	13.0	6500	176	179	0.98	606	3.39	0.28
Z16	130	110	10.0	3.50	1.18	11.0	4500	335	314	1.07	965	2.88	0.25
Z17	90	90	10.0	3.00	1.00	9.0	3000	281	273	1.03	846	3.01	0.25
Z18	100	120	10.0	3.00	0.83	12.0	4500	211	196	1.08	671	3.17	0.28
Z19	80	100	10.0	3.05	0.80	10.0	3000	261	253	1.03	830	3.18	0.27
Z20	80	100	10.0	2.50	0.80	10.0	3600	152	159	0.95	457	2.87	0.25
Z21	160	160	13.0	4.35	1.00	12.3	7000	411	418	0.98	1508	3.61	0.30
Z22	125	115	10.0	4.50	1.09	11.5	4000	549	533	0.99	2170	3.92	0.32
Z23	120	100	10.0	4.67	1.20	10.0	4500	352	708	0.50	2577	3.64	0.60
Z24	90	90	10.0	3.20	1.00	9.0	4000	174	315	0.55	1072	3.40	0.50
Z25	120	100	10.0	4.80	1.20	10.0	4000	457	758	0.60	2759	3.64	0.49
Z26	110	90	10.0	3.49	1.22	9.0	4000	252	389	0.65	1153	2.96	0.37
Z27	150	150	15.0	4.35	1.00	10.0	7000	351	501	0.70	1600	3.19	0.37
Z28	150	130	12.0	4.38	1.15	10.8	6000	381	508	0.75	1682	3.31	0.36
Z29	150	130	10.0	4.72	1.15	13.0	5750	437	547	0.80	2138	3.91	0.40
Z30	150	130	10.0	5.00	1.15	13.0	5000	631	746	0.85	2460	3.30	0.32
Z31	130	115	10.0	3.70	1.13	11.5	5000	309	341	0.90	1165	3.41	0.31
Z32	120	140	12.0	3.40	0.86	11.7	5500	280	255	1.10	834	2.97	0.27
Z33	100	120	10.0	3.40	0.83	12.0	4000	317	264	1.20	981	3.09	0.30
Z34	150	130	10.0	3.63	1.15	13.0	5500	371	285	1.30	942	2.54	0.27
Z35	140	110	10.0	3.38	1.27	11.0	4250	406	290	1.40	780	1.92	0.22
Z36	100	120	10.0	3.17	0.83	12.0	3750	337	224	1.50	780	2.32	0.28
Z37	140	110	10.0	3.18	1.27	11.0	4150	401	250	1.60	651	1.62	0.21
Z38	130	130	10.0	3.47	1.00	13.0	4500	432	254	1.70	913	2.11	0.29
Z39	100	100	10.0	3.15	1.00	10.0	2750	494	275	1.80	854	1.73	0.25
Z40	100	100	10.0	3.03	1.00	10.0	2750	475	251	1.90	756	1.59	0.25
Z41	150	130	10.0	3.06	1.15	13.0	5000	378	189	2.00	553	1.46	0.24

Table 2: Selected LC column geometries, buckling loads and relevant load ratios (dimensions in mm and loads in kN)

	b_w	b_f	b_l	t	$\frac{b_w}{b_f}$	$\frac{b_f}{b_l}$	L	P_{crG}	P_{crD}	R_{GD}	P_{crL}	$\frac{P_{crL}}{P_{cr,Max}}$	$\frac{P_{crL}}{P_{y,Max}}$
LC1	100	90	15.0	5.00	1.11	6.0	5000	211	1200	0.18	3591	2.99	1.39
LC2	120	80	10.0	5.00	1.50	8.0	7000	177	1034	0.16	3834	3.51	1.74
LC3	100	90	15.0	5.00	1.11	6.0	1550	1269	1273	1.00	3591	2.82	0.23
LC4	150	130	13.0	4.00	1.15	10.0	4150	434	436	1.00	1293	2.96	0.24
LC5	160	130	13.0	4.00	1.23	10.0	4500	427	435	0.98	1169	2.69	0.22
LC6	140	140	13.0	3.50	1.00	10.8	4500	290	293	0.99	869	2.97	0.24
LC7	140	160	15.0	4.00	0.88	10.7	4500	369	387	0.95	1165	3.01	0.26
LC8	150	150	15.0	4.00	1.00	10.0	4500	411	418	0.98	1240	2.97	0.25
LC9	170	150	15.0	4.50	1.13	10.0	4850	530	547	0.97	1621	2.96	0.25
LC10	180	150	15.0	5.00	1.20	10.0	4750	697	701	0.99	1967	2.81	0.23
LC11	120	120	10.0	3.00	1.00	12.0	4000	197	196	1.00	628	3.18	0.26
LC12	120	100	10.0	4.50	1.20	10.0	2500	671	650	1.03	2114	3.15	0.27
LC13	100	100	10.0	3.50	1.00	10.0	2500	348	351	0.99	1173	3.35	0.28
LC14	100	90	10.0	3.50	1.11	9.0	2250	399	395	1.01	1202	3.01	0.25
LC15	130	130	10.0	3.00	1.00	13.0	4750	177	179	0.99	585	3.27	0.27
LC16	130	110	10.0	3.50	1.18	11.0	3750	299	314	0.95	941	3.00	0.26
LC17	90	90	10.0	3.00	1.00	9.0	2250	270	276	0.98	810	2.94	0.24
LC18	100	120	10.0	3.00	0.83	12.0	3150	207	198	1.05	635	3.07	0.26
LC19	80	100	10.0	3.00	0.80	10.0	2000	266	248	1.07	764	2.87	0.25
LC20	80	100	10.0	2.50	0.80	10.0	2500	150	161	0.93	432	2.68	0.24
LC21	160	160	13.0	4.00	1.00	12.3	5150	370	343	1.08	1115	3.01	0.27
LC22	125	125	10.0	3.00	1.00	12.5	4250	203	187	1.08	604	2.98	0.26
LC23	120	100	10.0	4.50	1.20	10.0	3950	318	643	0.50	2250	3.50	0.58
LC24	90	90	10.0	3.00	1.00	9.0	3200	150	271	0.55	853	3.15	0.46
LC25	120	100	10.0	4.50	1.20	10.0	3500	386	644	0.60	2218	3.44	0.47
LC26	110	90	10.0	3.17	1.22	9.0	3500	200	308	0.65	841	2.73	0.34
LC27	150	150	15.0	4.00	1.00	10.0	5550	288	412	0.70	1199	2.91	0.34
LC28	150	130	12.0	4.06	1.15	10.8	5000	318	423	0.75	1310	3.10	0.34
LC29	150	130	10.0	4.20	1.15	13.0	5000	325	407	0.80	1459	3.58	0.37
LC30	130	110	10.0	3.50	1.18	11.0	4000	268	314	0.85	949	3.03	0.29
LC31	130	115	10.0	3.55	1.13	11.5	4000	278	309	0.90	994	3.22	0.29
LC32	120	140	12.0	3.02	0.86	11.7	4000	216	195	1.10	553	2.57	0.23
LC33	100	120	10.0	2.96	0.83	12.0	2900	230	192	1.20	603	2.62	0.26
LC34	150	130	10.0	2.90	1.15	13.0	4850	216	166	1.30	466	2.16	0.23
LC35	140	110	10.0	3.25	1.27	11.0	3500	369	264	1.40	675	1.83	0.21
LC36	100	120	10.0	3.15	0.83	12.0	2600	335	224	1.50	736	2.20	0.27
LC37	140	110	10.0	3.19	1.27	11.0	3300	404	253	1.60	629	1.56	0.20
LC38	130	130	10.0	3.13	1.00	13.0	3500	340	200	1.70	637	1.87	0.26
LC39	100	100	10.0	3.12	1.00	10.0	2000	492	273	1.80	824	1.67	0.25
LC40	100	100	10.0	2.98	1.00	10.0	2000	468	246	1.90	714	1.53	0.24
LC41	150	130	10.0	3.00	1.15	13.0	3850	362	181	2.00	498	1.38	0.23

Table 3: Selected WSLC column geometries, buckling loads and relevant load ratios (dimensions in mm and loads in kN)

	b_w	b_f	b_l	t	$\frac{b_w}{b_f}$	$\frac{b_f}{b_l}$	L	P_{crG}	P_{crD}	R_{GD}	P_{crL}	$\frac{P_{crL}}{P_{cr,Max}}$	$\frac{P_{crL}}{P_{y,Max}}$
WSLC1	100	90	15.0	5.00	1.11	6.0	5000	224	1212	0.18	5606	4.63	2.04
WSLC2	120	80	10.0	5.00	1.50	8.0	7000	191	1185	0.16	5831	4.92	2.50
WSLC3	100	90	15.0	5.00	1.11	6.0	1550	1327	1297	1.02	4876	3.68	0.31
WSLC4	150	130	13.0	4.00	1.15	10.0	4150	449	442	1.02	1803	4.02	0.33
WSLC5	160	130	13.0	4.00	1.23	10.0	4500	440	441	1.00	1862	4.22	0.35
WSLC6	140	140	13.0	3.55	1.00	10.8	4500	305	306	1.00	1106	3.61	0.30
WSLC7	140	160	15.0	4.00	0.88	10.7	4500	379	390	0.97	1288	3.30	0.28
WSLC8	150	150	15.0	4.00	1.00	10.0	4500	423	420	1.01	1444	3.42	0.28
WSLC9	170	150	15.0	4.50	1.13	10.0	4850	545	551	0.99	2145	3.90	0.32
WSLC10	180	150	15.0	5.00	1.20	10.0	4750	715	708	1.01	2855	3.99	0.33
WSLC11	120	120	10.0	3.00	1.00	12.0	4000	206	201	1.02	800	3.89	0.32
WSLC12	120	100	10.0	4.50	1.20	10.0	2500	703	673	1.05	3507	4.99	0.43
WSLC13	100	100	10.0	3.50	1.00	10.0	2500	366	361	1.02	1494	4.08	0.34
WSLC14	100	90	10.0	3.50	1.11	9.0	2250	422	410	1.03	1719	4.07	0.34
WSLC15	130	130	10.0	3.00	1.00	13.0	4750	184	183	1.01	744	4.04	0.33
WSLC16	130	110	10.0	3.50	1.18	11.0	3750	312	324	0.96	1494	4.61	0.39
WSLC17	90	90	10.0	3.00	1.00	9.0	2250	287	285	1.01	1032	3.59	0.30
WSLC18	100	120	10.0	3.00	0.83	12.0	3150	216	202	1.07	736	3.40	0.30
WSLC19	80	100	10.0	3.05	0.80	10.0	2000	288	264	1.09	905	3.14	0.28
WSLC20	80	100	10.0	2.50	0.80	10.0	2500	159	165	0.97	496	3.00	0.25
WSLC21	125	125	10.0	3.00	1.00	12.5	4250	203	192	1.06	768	3.77	0.33
WSLC22	160	160	13.0	4.00	1.00	12.3	5150	380	347	1.10	1394	3.67	0.33
WSLC23	120	100	10.0	4.50	1.20	10.0	3950	335	664	0.50	3755	5.66	0.92
WSLC24	90	90	10.0	3.12	1.00	9.0	3200	169	306	0.55	1235	4.03	0.60
WSLC25	120	100	10.0	4.55	1.20	10.0	3500	412	683	0.60	3824	5.60	0.76
WSLC26	110	90	10.0	3.20	1.22	9.0	3500	214	328	0.65	1404	4.29	0.54
WSLC27	150	150	15.0	4.05	1.00	10.0	5550	301	428	0.70	1544	3.61	0.42
WSLC28	150	130	12.0	4.13	1.15	10.8	5000	337	448	0.75	2076	4.63	0.50
WSLC29	150	130	10.0	4.24	1.15	13.0	5000	341	427	0.80	2347	5.49	0.56
WSLC30	130	110	10.0	3.55	1.18	11.0	4000	285	335	0.85	1576	4.71	0.45
WSLC31	130	115	10.0	3.60	1.13	11.5	4000	295	329	0.90	1543	4.69	0.43
WSLC32	120	140	12.0	3.09	0.86	11.7	4000	230	209	1.10	687	2.99	0.27
WSLC33	100	120	10.0	3.03	0.83	12.0	2900	248	207	1.20	745	3.01	0.29
WSLC34	150	130	10.0	3.01	1.15	13.0	4850	243	186	1.30	786	3.23	0.34
WSLC35	140	110	10.0	3.26	1.27	11.0	3500	386	276	1.40	1210	3.13	0.36
WSLC36	100	120	10.0	3.22	0.83	12.0	2600	360	240	1.50	892	2.48	0.30
WSLC37	140	110	10.0	3.20	1.27	11.0	3300	422	264	1.60	1133	2.68	0.35
WSLC38	130	130	10.0	3.16	1.00	13.0	3500	357	209	1.70	843	2.36	0.33
WSLC39	100	100	10.0	3.19	1.00	10.0	2000	533	296	1.80	1101	2.07	0.30
WSLC40	100	100	10.0	3.05	1.00	10.0	2000	508	267	1.90	958	1.89	0.29
WSLC41	150	130	10.0	3.02	1.15	13.0	3850	378	189	2.00	768	2.04	0.33

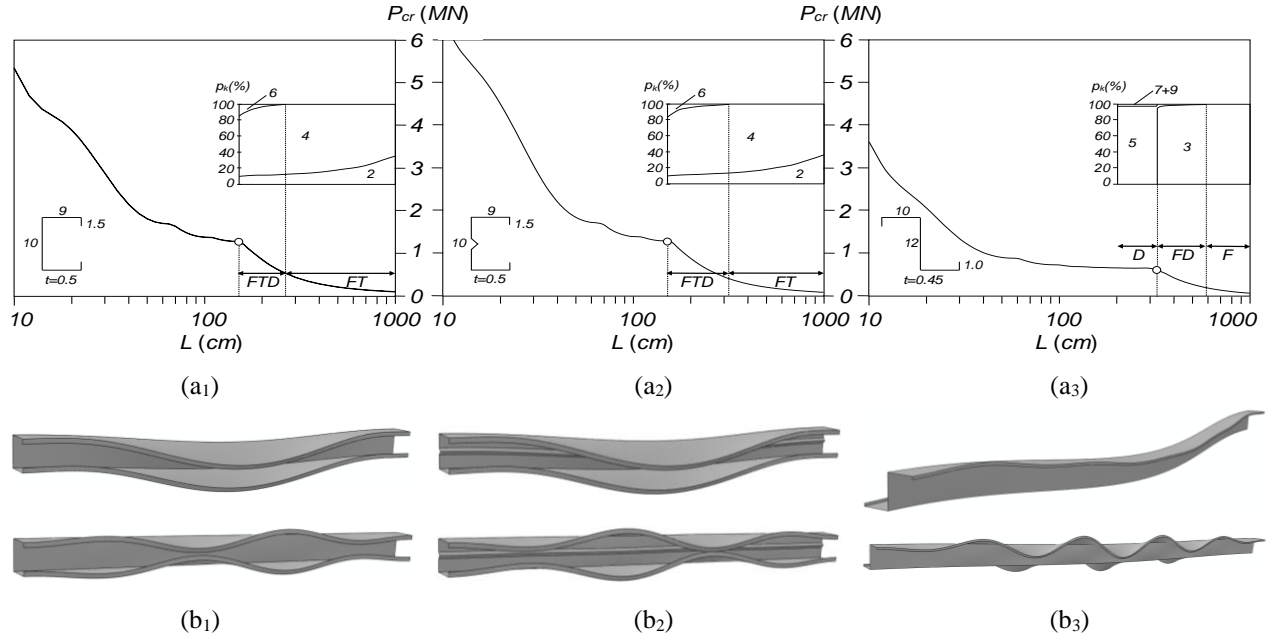


Figure 1: (a) P_{cr} vs. L curves and modal participation diagrams and (b) critical “global” and distortional mode shapes (top and bottom figures), for (1) LC, (2) WSLC and (3) Z columns.

(sometimes between quotation marks, when confusion may arise). The longer columns buckle in the (expected) flexural-torsional (FT) modes, combining deformation modes 2 and 4 – truly global buckling. Note that the participation of mode 6 gradually decreases with L up to 250cm or 300cm (LC or WSLC columns), when FTD buckling switches to FT buckling. Therefore, the interaction between distortional and “global” is always associated with the FTD buckling mode since (ii₁) the difference between the distortional and FT buckling loads is quite substantial and (ii₂) the post-critical strength associated with FT buckling is too small to allow for such interaction. However, as reported by Martins *et al.* (2016c), the participation of mode 6 becomes gradually less relevant as post-buckling progresses.

- (ii) The GBT modal participation diagrams concerning the Z columns show that, for lengths in the close vicinity of the transition between critical distortional and global buckling, the column global critical buckling mode involves not only the expected and predominant minor-axis flexure, but also a tiny (but clearly visible in Fig. 1(b₃)) contribution from the symmetric distortional mode 5 (it is, in fact, a FD mode). Once again, the expected truly global (minor-axis flexure) buckling mode is observed only for the longer columns ($L > 600$ cm).
- (iii) The practical coincidence between P_{crD} and P_{crG} (see Tables 1-3) implies that the post-buckling behavior and strength are certainly affected by strong D-G interaction.

3. Post-Buckling Behavior of Columns Affected by Distortional-Global Interaction

3.1 Elastic Geometrically Non-Linear Behavior

This section addresses the elastic non-linear post-buckling behavior of columns affected by D-G interaction and begins by investigating the influence of the initial geometrical imperfection shape. The study is restricted to columns with practically coincident critical distortional and “global” buckling loads ($R_{GD} \cong 1.0$ – highest D-G interaction effects). Moreover, only linear combinations of “pure” distortional and global buckling modes shapes are considered, combining arbitrarily the two normalised buckling

modes and sharing the same overall amplitude – the Z columns results are presented first, followed by those concerning WSLC columns (the LC column results were previously reported by Dinis & Camotim 2011a and Camotim & Dinis 2013).

Two different Z columns are considered in this study – the major difference between them concerns the critical distortional half-wave number (n_D): columns Z6 ($R_{GD}=0.95$) and Z13 ($R_{GD}=0.94$) exhibit an even and odd n_D , respectively. They contain initial imperfections combining 10 or 9 D half-waves with 1 “global” half-wave. In order to obtain column equilibrium paths that (i) cover the whole imperfection shape range and (ii) can be meaningfully compared, the following approach is adopted:

- (i) Determination of “pure” critical buckling mode shapes, normalized to exhibit unit maximum flange-lip corner vertical displacement ($v_D=1$ or $v_G=1$) – see Fig. 2(a) for the Z6 column.
- (ii) Then, a given “combined” imperfection shape is obtained as a linear combination of the pure D and G modes, with coefficients $v_{G,90}$ and $v_{D,0}$ lying on the ellipse shown in Fig. 2(a) and covering every possible combination. Each selected initial imperfection shape lies on this ellipse and corresponds to an angle θ , measured counter-clockwise from the $v_{D,0}$ axis, so that $v_{D,90}=r\sin\theta$ and $v_{D,0}=r\cos\theta$, where r is the ellipse polar coordinate. The amplitudes of the “pure” distortional ($\theta=0^\circ$ or 180° – Fig. 2(b)) and “global” ($\theta=90^\circ$ or 270° – Fig. 2(b)) are equal to $0.94t$ (corresponding to a 50% probability that a random imperfection amplitude is below this value – see Schafer & Peköz 1998a) and $L/1000$, respectively. A total of 24 initial imperfections shapes are considered (15° θ intervals, starting at 0°).

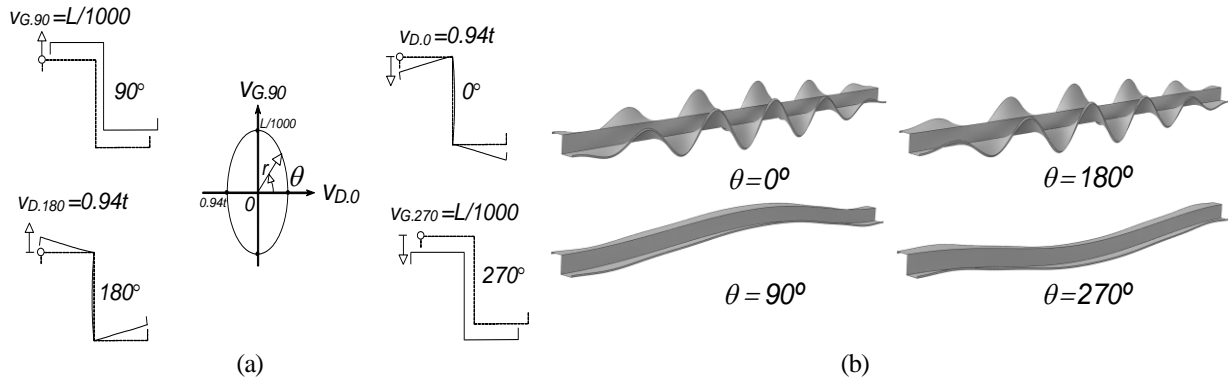


Figure 2: Initial imperfection (a) $v_{D,90}$ - $v_{G,0}$ plane representation and (b) $\theta=0^\circ, 90^\circ, 180^\circ, 270^\circ$ shapes – Z6 column (even n_D)

To assess how the imperfection shape influences the post-buckling behavior of the two Z columns affected by D-G interaction, numerical equilibrium paths concerning columns with the various initial imperfections are presented and discussed – such paths are hereafter identified by their θ values. Figs. 3(a)-(b) show elastic equilibrium paths P/P_{cr} vs. $(v+v_0)/t$ (v is the mid-span top flange-lip corner vertical displacement and v_0 the corresponding initial value) of $\theta=0^\circ, 15^\circ, \dots, 345^\circ$ Z6 and Z13 columns. Moreover, Fig. 3(c) shows several deformed configurations at advance post-buckling stages (discussed below). The observation of all these post-buckling results leads to the followings conclusions:

- (i) Most equilibrium paths in Fig. 3(a)-(b) show deformed configurations combining a predominant “global” (minor-axis flexure) half-wave with several distortional half-waves, thus evidencing the occurrence of D-G interaction. For instance, Figs. 3(c₁)-(c₂) show the deformed configurations of the Z6+ $\theta=90^\circ$ and Z6+ $\theta=270^\circ$ columns at advanced post-buckling stages ($(v+v_0)/t=30$). As expected, the post-critical strengths and failure loads ($P_U/P_{cr}<1.0$) of these columns are very small.
- (ii) The equilibrium paths displayed in Fig. 3(a), concerning a Z column with an even n_D , can be divided into three groups: (ii₁) $\theta=0^\circ$ and $\theta=180^\circ$ (discussed in the next item), (ii₂) $195^\circ \leq \theta \leq 345^\circ$, associated

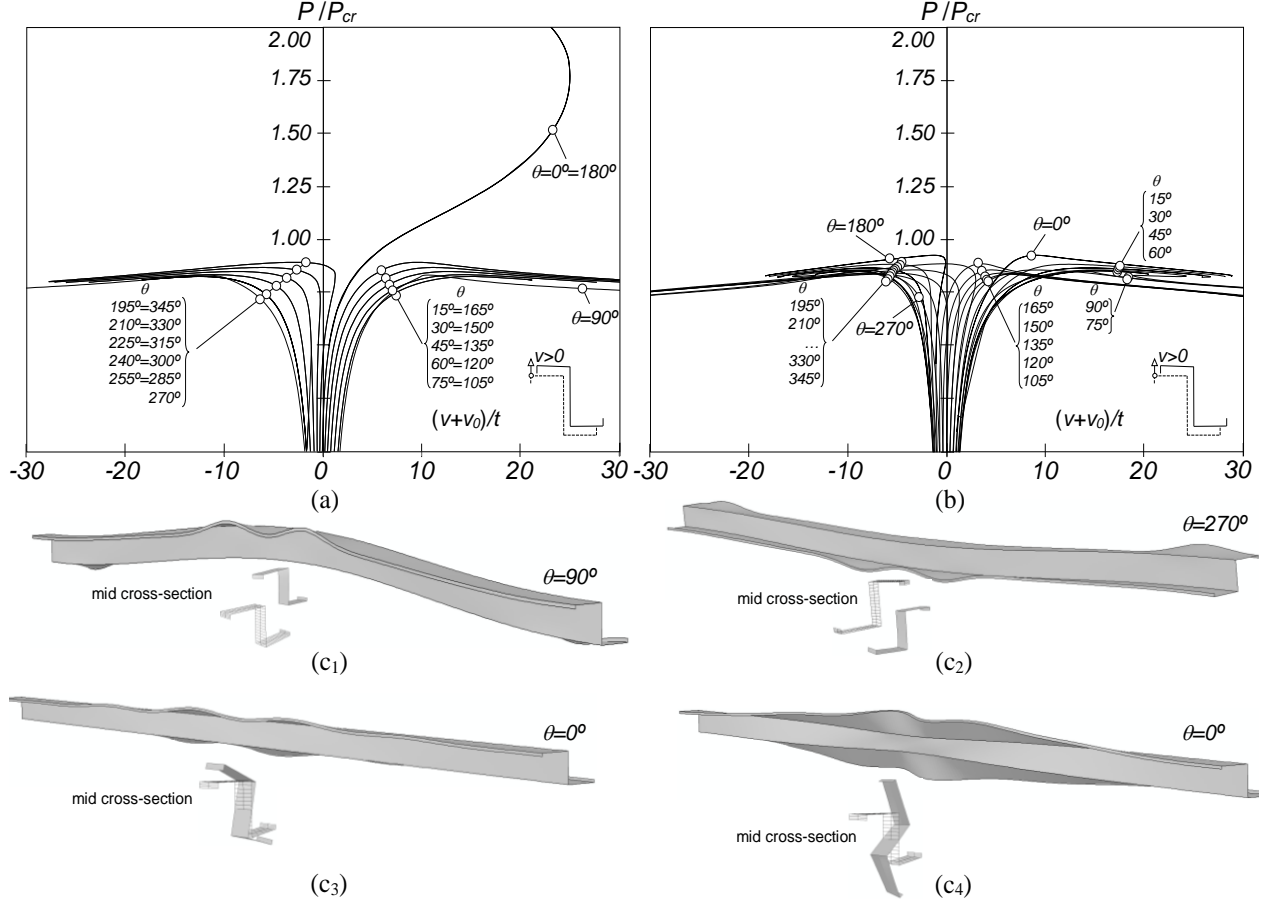


Figure 3: Elastic post-buckling equilibrium paths P/P_{cr} vs. $(v+v_0)/t$ of Z columns with (a) even and (b) odd critical distortional half-waves, and (c) deformed configurations at advanced post-buckling stages of the columns (c₁) Z6+ $\theta=90^\circ$, at $(v+v_0)/t=30$, (c₂) Z6+ $\theta=270^\circ$, at $(v+v_0)/t=30$, (c₃) Z6+ $\theta=0^\circ$, at $(v+v_0)/t=10$, and (c₄) Z6+ $\theta=0^\circ$, at $(v+v_0)/t=25$

with minor-axis flexural deformations towards the bottom flange (hereafter denoted “negative”) and (ii₃) all the remaining ones ($15^\circ \leq \theta \leq 165^\circ$), involving almost exclusively “positive” minor-axis flexural deformations. On the other hand, Z columns with an odd n_D exhibit two “common curves”⁹ – the $\theta=0^\circ$ and $\theta=180^\circ$ equilibrium paths are included in the groups $0^\circ \leq \theta \leq 165^\circ$ and $180^\circ \leq \theta \leq 345^\circ$, respectively. Note that different initial imperfection amplitudes may lead to significant differences in the features of the column post-buckling behavior (see, for instance, Dinis & Camotim 2011a).

- (iii) Surprisingly, the two equilibrium paths of columns with an even n_D and containing pure distortional imperfections ($\theta=0^\circ$ and $\theta=180^\circ$) are clearly different from those exhibited by all the remaining columns. Figs. 3(c₃)-(c₄) show deformed configurations at two post-buckling stages of these columns ($(v+v_0)/t=10$ and 25). These figures provide evidence that these columns are affected by a different nature of D-G interaction, involving distortional deformations and torsional rotations – distortional-torsional interaction. Note that this D-T interaction is not due to the closeness between the distortional and torsional buckling loads. In fact, unpublished GBT-based results show that torsional rotations may emerge in columns affected by D-G interaction exhibiting a pure distortional post-buckling

⁹ Rigorously speaking, there are four different common curves, each corresponding to the equilibrium paths (θ) belonging to the same quadrant. For instance, the equilibrium paths $105^\circ \leq \theta \leq 165^\circ$ do not merge with that common to the $0^\circ \leq \theta \leq 90^\circ$ ones, because of the distortional imperfection different sign (recall the asymmetry with respect to the flange-lip motions – e.g., Silvestre & Camotim 2003). The same applies to the $195^\circ \leq \theta \leq 270^\circ$ and $285^\circ \leq \theta \leq 345^\circ$ equilibrium paths. Since this asymmetry is fairly mild, it was considered to group all of them together.

behavior, even when the critical torsional ($P_{cr,T}$) and minor-axis flexural ($P_{cr,F}$) buckling loads are not too close – such situation “attracts”/favours the interaction with torsional buckling. If $P_{cr,T}/P_{cr,F}$ is high enough, the above D-T interaction does not occur – this is the case of the Z13 column (see Fig. 3(b)). Note that this type of D-G interaction cannot occur in (“very long”) columns buckling in torsional modes – in such columns, the critical distortional buckling load is much higher than $P_{cr,T}$.

- (iv) Since all equilibrium paths exhibit limit points prior to merging into “common curves” (except those addressed in the previous item), the most detrimental initial imperfection can be easily identified: that leading to the lowest failure load. Fig. 3(a) shows that the $\theta=75^\circ; 105^\circ; 255^\circ; 285^\circ$ initial imperfections are the most detrimental (they correspond to $P_U/P_{cr}=0.825$). In Fig. 3(b), on the other hand, this role is played by the $\theta=120^\circ; 300^\circ$ initial imperfections, which correspond to $P_U/P_{cr}=0.838$. Nevertheless, it should be mentioned that P_U/P_{cr} is practically the same for the columns containing pure “global” initial imperfections – therefore, for the sake of simplicity, it is assumed, in the remainder of this work, that the pure “global” initial imperfection is the most detrimental one.

A similar investigation was performed for WSLC columns and, once again, two columns differing in the n_D nature (even or odd) were considered: WSLC6 ($R_{GD}=1.00$ and odd n_D) and WSLC14 ($R_{GD}=1.03$ and even n_D). Fig. 4(a), similar to Fig. 2(a), shows all the possible initial imperfection shapes and Fig. 4(b) displays the WSLC6 column two pure distortional ($\theta=0^\circ$ and $\theta=180^\circ$ – 7 half-waves) and two pure “global” ($\theta=90^\circ$ and $\theta=270^\circ$) initial imperfections. On the other hand, Figs. 5(a)-(b) show the elastic equilibrium paths P/P_{cr} vs. $(v+v_0)/t$ of both columns (WSLC6 and WSLC14) with $\theta=0^\circ, 15^\circ, \dots, 345^\circ$ initial imperfections – Fig. 5(c) depicts several deformed configurations at advance post-buckling stages. The observation of all these post-buckling results prompts the following comments:

- (i) The equilibrium paths displayed at Fig. 5(a)-(b) can be divided into three or four groups, depending on the nature of n_D , but they only correspond to two distinct post-buckling behavior mechanics: (i₁) $15^\circ < \theta < 165^\circ + 195^\circ < \theta < 345^\circ$, and (i₂) $\theta=0^\circ + 180^\circ$.
- (ii) The first behavior ($15^\circ < \theta < 165^\circ + 195^\circ < \theta < 345^\circ$) is associated with the vast majority of equilibrium paths and combines predominantly counter-clockwise ($15^\circ < \theta < 165^\circ$) or clockwise ($195^\circ < \theta < 345^\circ$) rotations¹⁰ with distortional deformations. Therefore, these columns are affected by the “expected” interaction between the distortional and FTD buckling modes – Figs. 5(c₁)-(c₂) show the $\theta=90^\circ$ and $\theta=270^\circ$ WSLC6 column deformed configurations at $(v+v_0)/t=50$. Moreover, note that the equilibrium

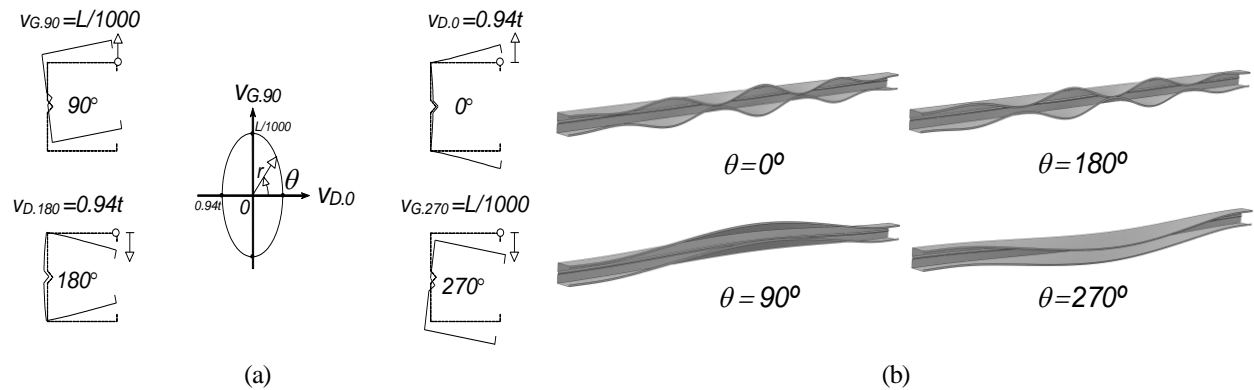


Figure 4: Initial imperfection (a) $v_{D,90}$ - $v_{G,0}$ plane representation and (b) $\theta=0^\circ, 90^\circ, 180^\circ, 270^\circ$ shapes – WSLC6 column (odd n_D)

¹⁰ In fact, as seen in Section 2, the “global” buckling mode contains (i) torsional, (ii) major-axis flexural and (iii) anti-symmetric distortional contributions – the torsional one is the most relevant (see also Martins *et al.* 2016c).

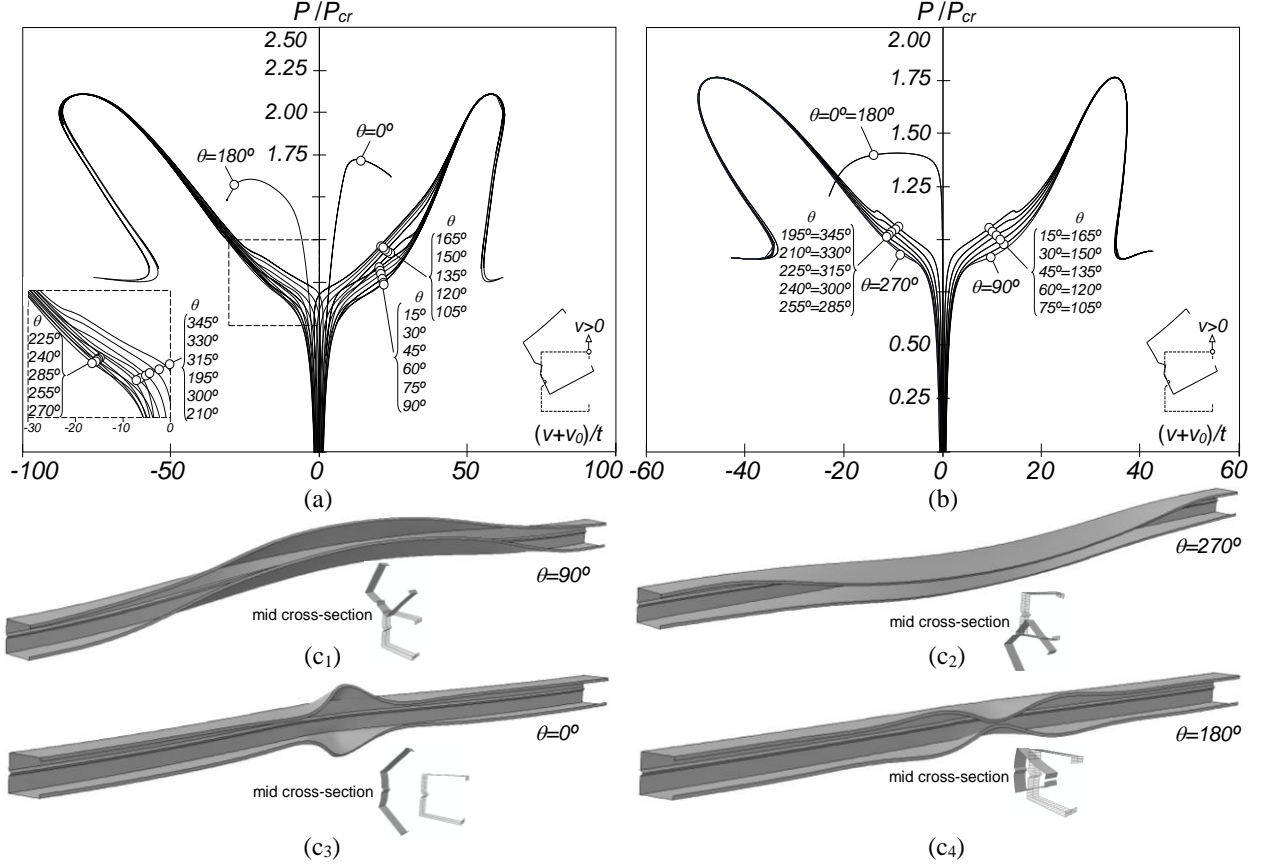


Figure 5: WSLC-column elastic post-buckling equilibrium paths P/P_{cr} vs. $(v+v_0)/t$ with (a) odd and (b) even critical distortional half-waves numbers and (c) deformed configurations at advanced post-buckling stages concerning (c₁) WSLC6+ $\theta=90^\circ$ at $(v+v_0)/t=50$, (c₂) WSLC6+ $\theta=270^\circ$ at $(v+v_0)/t=50$, (c₃) WSLC6+ $\theta=0^\circ$ at $(v+v_0)/t=25$ and (c₄) WSLC6+ $\theta=180^\circ$ at $(v+v_0)/t=15$

paths $\theta=15^\circ, \dots, 165^\circ$ and $\theta=195^\circ, \dots, 345^\circ$ are symmetric with respect to the sign of the “global” initial imperfection, even if this symmetry is not reflected in Figs. 5(a)-(b). This is due to the contribution of the anti-symmetric distortional mode **6** (if the $\theta=195^\circ, \dots, 345^\circ$ equilibrium paths involved the mid-span bottom flange-lip corner vertical displacement, they would reflect the above symmetry).

- (iii) Once again, the $\theta=0^\circ$ and $\theta=180^\circ$ equilibrium paths correspond to mechanically distinct post-buckling behaviors – Figs. 5(c₃)-(c₄) show the deformed configurations of the $\theta=0^\circ$ and $\theta=180^\circ$ WSLC6 columns at $(v+v_0)/t=25$ and $(v+v_0)/t=15$, respectively, including the mid-span deformed cross-sections. These configurations combine distortional and minor-axis flexural deformations, which evidences the presence of a different nature of D-G interaction. Similar observations were made, in the context of LC columns, by Dinis & Camotim (2011a), Camotim & Dinis (2013) and, recently, Martins *et al.* (2016c) – these last authors performing GBT analyses. In addition, Dinis & Camotim (2010, 2011b) also investigated rack-section and lipped channel columns undergoing L-D-G interaction. They showed that minor-axis flexural deformations emerge due to the stress redistribution caused by the distortional deformations and, subsequently (at advanced post-buckling stages), trigger the interaction with minor-axis flexural buckling¹¹. Moreover, and like in the $\theta=0^\circ$ and $\theta=180^\circ$ Z columns, this type of interaction cannot occur for (“very long”) columns with critical minor-axis flexural buckling modes, since the distortional buckling load is much higher than

¹¹ Naturally, this type of interaction is also shared by columns made with singly symmetric cross-sections.

the minor-axis flexural one. Fig. 5(a) also shows an asymmetry regarding the sign of the distortional initial imperfection: the $\theta=0^\circ$ (mid-span outward flange-lip motions) exhibits higher strengths – naturally, such asymmetry does not exist when n_D is even (see Fig. 5(b)).

- (iv) The most detrimental initial geometrical imperfection shape, in the sense that it maximizes the column strength erosion, is the pure “global” one ($\theta=90^\circ$ or $\theta=270^\circ$) – the corresponding equilibrium paths lie below all the remaining ones.
- (v) All the equilibrium paths shown in Figs. 5(a)-(b), associated with columns undergoing distortional-FTD interaction, exhibit much higher post-critical strength than those obtained for the Z columns, which are affected by distortional-F (minor-axis flexure) interaction (see Figs. 3(a)-(b)).
- (vi) Finally, it should be mentioned that the (vi₁) WSLC and LC columns undergoing distortional-F (minor-axis flexure) interaction and (vi₂) Z columns affected by distortional-T (torsional) interaction correspond clearly to singular post-buckling behaviors and are very unlikely (or even impossible) to occur in “real” columns. Therefore, the further investigation on columns affected by D-G interaction (relevance and design) focuses the behaviors likely to occur in practice, *i.e.*, either to distortional-FTD (LC and WSLC columns) or distortional-F (minor-axis flexure) (Z columns) interaction.

3.2 Relevance of D-G Interaction

In order to assess the relevance of D-G interaction in CFS columns, it is essential to gather a substantial numerical failure load data concerning columns with (i) various R_{GD} values and (ii) wide range of critical (distortional or global) slenderness values λ_{cr} , in order to capture possible “secondary-bifurcation D-G interactions” – 11 different values are considered, namely $\lambda_{cr}=\{0.50,0.75,1.00,1.25,1.50,1.75,2.00,2.50,3.00,3.25,3.50\}$. The methodology adopted in this investigation is very similar to that followed in the context of the L-D interaction in CFS columns (Martins *et al.* 2015) and involves the the following steps:

- (i) Identify the R_{GD} range associated with “true D-G interaction” (Martins *et al.* 2016c), for which the distortional and “global” buckling loads (“intrinsic” to the column) are fairly close – this type of interaction always occurs.
- (ii) Identify minimum $R_y=P_y/\max(P_{crD};P_{crG})$ values allowing for the development of “secondary-bifurcation (distortional or global) D-G interaction” (if possible). This type of interaction may occur for R_{GD} values significantly different from 1.0, provided that the yield stress is sufficiently high to enable the interaction to develop. Naturally, the “secondary-global bifurcation D-G interaction” is more likely to occur, due to the higher post-critical strength reserve exhibited by columns buckling in distortional modes. However, since the LC and WSLC columns with moderate-to-long slenderness were shown to exhibit also a non-negligible “global” post-critical strength reserve, “secondary-distortional bifurcation D-G interaction” may also occur in such columns.

3.2.1 True D-G interaction

The elastic-plastic post-buckling behavior and strength of Z, WSLC and LC columns undergoing “true D-G interaction” is first addressed. Figs. 6(a₁)-(a₃) show P_{cr} vs. $(v+v_0)/t$ equilibrium paths of Z11, WSLC5 and LC6 columns with $R_{GD}=1.0$, 5 critical slenderness values (1.0, 2.0, 3.0, 3.5, ∞ – the last stands for the elastic behavior) and containing pure “global” initial imperfections. On the other hand, Figs. 6(b₁)-(b₃) display deformed configurations and plastic strain diagrams at the onset of collapse concerning the aforementioned four elastic-plastic columns. The observation of the results presented in these figures prompts the following remarks:

- (i) All Z columns exhibit distortional and (mostly) minor-axis flexural deformations combined since the early loading stages (see the deformed configuration at collapse of the $\lambda_{cr}=1.0$ column depicted in

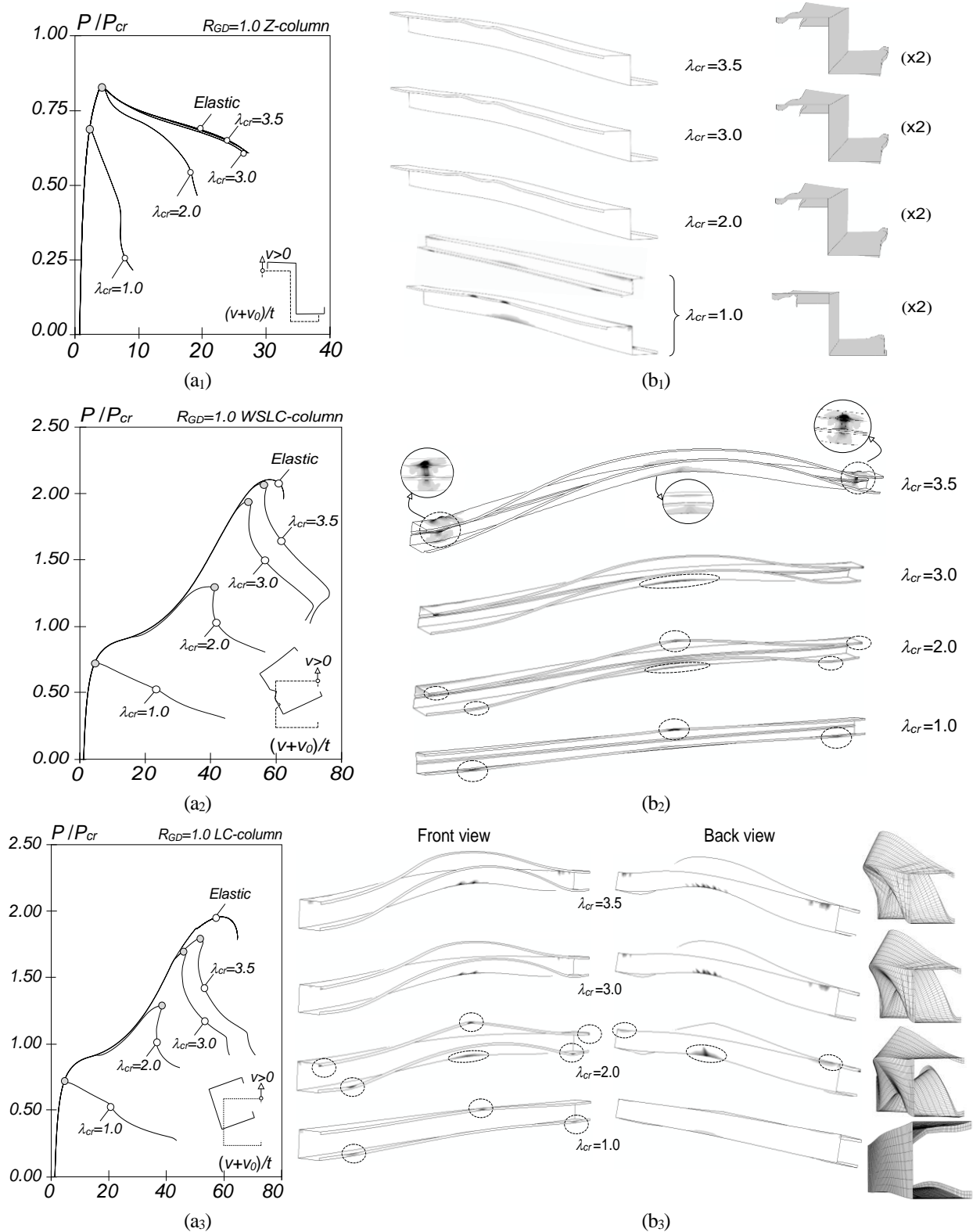


Figure 6: (a) Elastic and elastic-plastic P/P_{cr} vs. $(v+v_0)/t$ equilibrium paths and (b) deformed configurations at the onset of collapse for (1) Z11, (2) WSLC6 and (3) LC6 columns undergoing “true D-G interaction” with $\lambda_{cr}=1.0, 2.0, 3.0$ and 3.5

Fig. 6(b₁)), which characterizes the “true D-G interaction”. On the other hand, the WSLC and (mostly) LC columns also exhibit distortional and FTD deformations also since the early loading stages (see also item (iii₃) below) – however, the latter are barely visible in Fig. 6(b₁) due to the presence of anti-symmetric distortion (mode 6) in the “global” buckling mode – this issue will be further discussed in Section 3.2.2.

- (ii) With the exception of the stockiest one ($\lambda_{cr}=1.0$), all Z columns remain elastic until the failure load is reached – moreover, the elastic limit point falls below the critical buckling load. The Z11+ $\lambda_{cr}=1.0$ column exhibits a very small elastic-plastic strength reserve¹² – as shown in Fig. 6(b₁), yielding starts at the (ii₁) lip-bottom flange and web-top flange end regions, and (ii₂) web-bottom flange and lip-top flange mid-span regions.
- (iii) The failure modes of the LC and WSLC are very similar and can be divided into three groups, according to the critical slenderness value:
 - (iii₁) The stocky columns (*e.g.*, $\lambda_{cr}=1.0$) collapse abruptly after the yielding of the top flange-lip mid-span region and bottom flange-lip assembly end regions (see Figs. 6(b₂)-(b₃)).
 - (iii₂) In the columns with $\lambda_{cr}\cong 2.0$ yielding starts in the same areas identified in the previous item and is followed by a pronounced elastic-plastic strength reserve (see Fig. 6(a₂)-(a₃)). Collapse occurs after the yielding of the web-bottom flange mid-span region (see Fig. 6(b₂)-(b₃)).
 - (iii₃) The columns with $\lambda_{cr}>2.0$ exhibit a minute elastic-plastic strength reserve and practically all of them collapse after the yielding of the lip-bottom flange mid-span region and web-top flange end regions. The exceptions are the $\lambda_{cr}=3.0$ and 3.5 LC columns, as illustrated in Fig. 6(b₃) – this is because these columns exhibit also local deformations, *i.e.*, undergo L-D-G interaction. Indeed, it was very difficult to select LC column geometries having the local critical buckling load much higher than its distortional and global counterparts (see Table 2), *i.e.*, to preclude the occurrence of L-D-G interaction. In order to overcome this difficulty, it was decided to analyze WSLC columns in this work (the local critical buckling load is much higher).

3.2.2 Secondary-distortional bifurcation D-G interaction

Figs. 7(a)-(c) display elastic and elastic-plastic equilibrium paths of the Z23, WSLC23 and LC23 columns, which have $R_{GD}=0.5$ and exhibit typical global post-buckling behaviors. The observation of these figures shows that, as already mentioned in Section 3.1, the post-critical strength is small in the Z columns¹³ and high in the WSLC and LC columns¹⁴. Therefore, the occurrence of “secondary-distortional bifurcation D-G interaction” (SDI) is (i) very unlikely in the Z columns and (ii) quite possible in the WSLC and LC columns – the illustration of this assertion is address next, first for the Z columns.

Figs. 8(a)-(f) show the failure modes of Z columns with several R_{GD} values, all sharing the same “global” slenderness ($\lambda_G=3.5$) – they all fail in the elastic range (like all the columns with $\lambda_G>2.0$). Recalling that the “global” buckling mode contains a small contribution the symmetric distortional mode 5 (see Section 2 and Fig. 1(b₃)), the observation of these figures leads to the following comments:

- (i) The columns with $0.50 \leq R_{GD} \leq 0.85$ fail in “global” (FD) modes, which means that SDI does not develop – the distortional deformations appearing in the failure mode are not akin to the critical

¹² This very small elastic-plastic strength reserve is not perceptible in Fig. 6(a₁). Due to the horizontal scale, it is virtually impossible to distinguish between the elastic and elastic-plastic portions of the $\lambda_{cr}=1.0$ column equilibrium paths.

¹³ But higher than that of the Z columns undergo “true D-G interaction” – compare Figs. 7(a) and Fig. 6(a₁).

¹⁴ No comparison can be made with the WSLC and LC columns post-buckling behaviors displayed in Fig. 6(a₂)-(a₃) – recall that the post-buckling behavior of columns with these cross-sections are strongly dependent on their dimensions (see Section 4.2).

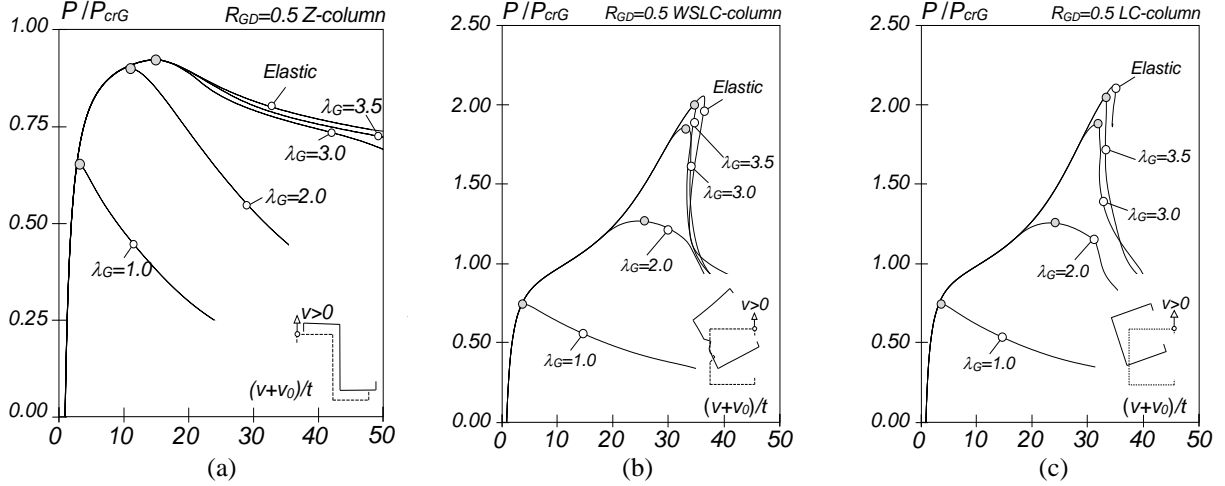


Figure 7: P/P_{cr} vs. $(v+v_0)/t$ equilibrium paths of (a) Z23, (b) WSLC23, (c) LC23 columns with $\lambda_G=1.0, 2.0, 3.0, 3.5, \infty$ (“global” post-buckling behavior)

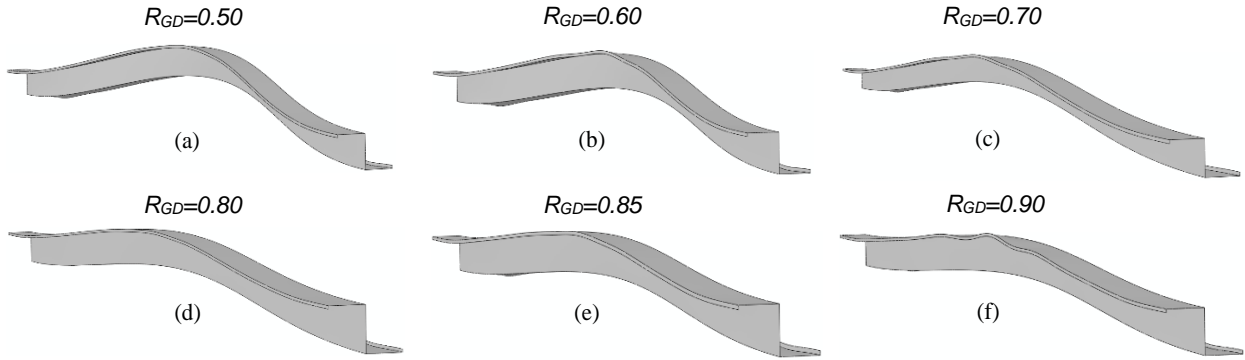


Figure 8: Failure modes of Z columns with $\lambda_G=3.5$ and (a) $R_{GD}=0.50$, (b) $R_{GD}=0.60$, (c) $R_{GD}=0.70$, (d) $R_{GD}=0.80$, (e) $R_{GD}=0.85$ and (f) $R_{GD}=0.90$ (all amplified 3 times)

distortional buckling mode (they stem from the “global” buckling mode). Note that the $R_{GD}=0.50$ column collapses with no trace of distortional deformation, because its “global” buckling mode is truly global (F – minor axis flexural) – see Fig. 1(a₃).

- (ii) Only the $R_{GD}=0.90$ Z column exhibit D-G interaction (see Fig. 8(f)). Thus, it may be argued that, in Z columns, D-G interaction only occurs when R_{GD} reaches a value between 0.85 and 0.90 – in this case, it is termed “true D-G interaction”.

Next, a similar investigation is conducted for WSLC columns. In such columns (singly symmetric cross-section) the possible (but unlikely) occurrence SDI interaction is very difficult to detect by observing the deformed configuration evolution. This is because (i) the “global” buckling mode contains a significant amount of anti-symmetric distortion (mode 6 – see Fig. 1(a₂)) and (ii) the interaction can only develop in advanced post-buckling stages, when torsion (mode 4) plays a major role (see, for instance, Fig. 5(c₁)), making the detection of symmetric distortional deformations (mode 5, which appears in the distortional buckling mode) an extremely difficult task. In order to overcome this difficulty, this study focuses on mid-web transverse displacement profiles, thus eliminating the contribution from the anti-symmetric distortional mode to the column structural response (this deformation mode exhibits double curvature in the web – e.g., see Camotim & Dinis 2013). Fig. 9 shows these displacement profiles for WSLC columns

with $R_{GD}=0.50, 0.60, 0.70, 0.80, 0.85, 0.90$ at several post-buckling stages, namely $P/P_{crG} \cong 1.00, 1.25, 1.50, 1.75, 2.00$ and peak load. The observation of these displacement profiles prompts the following remarks:

- (i) All the $R_{DG}=0.50$ column displacement profiles show one dominant half-wave, due to the torsion mode contribution (see Martins *et al.* 2016c), *i.e.*, this column post-buckling behavior is “global”.
- (ii) The displacement profiles of the (ii₁) $R_{GD}=0.60$ column at $P/P_{crG}=1.941$ (peak load) and (ii₂) $R_{GD}=0.70$ column at $P/P_{crG}=2.237$ (peak load) show minute “irregularities” in the predominantly single half-wave configuration, thus evidencing the presence of symmetric distortional deformations, *i.e.*, SDI interaction. These “irregularities” become perceptible at progressively lower applied load levels in the remaining columns – for instance, compare the displacement profile of the $R_{GD}=0.80$ column at $P/P_{crG}=1.985$ with that of the $R_{GD}=0.85$ column at $P/P_{crG}=1.750$.
- (iii) It will be shown later, in Section 4.3, that the global strength curve is able to handle adequately both the global and SDI failures. Therefore, is not necessary to establish any “border” between “global” and SDI failures – this assertion also applies to the LC columns.

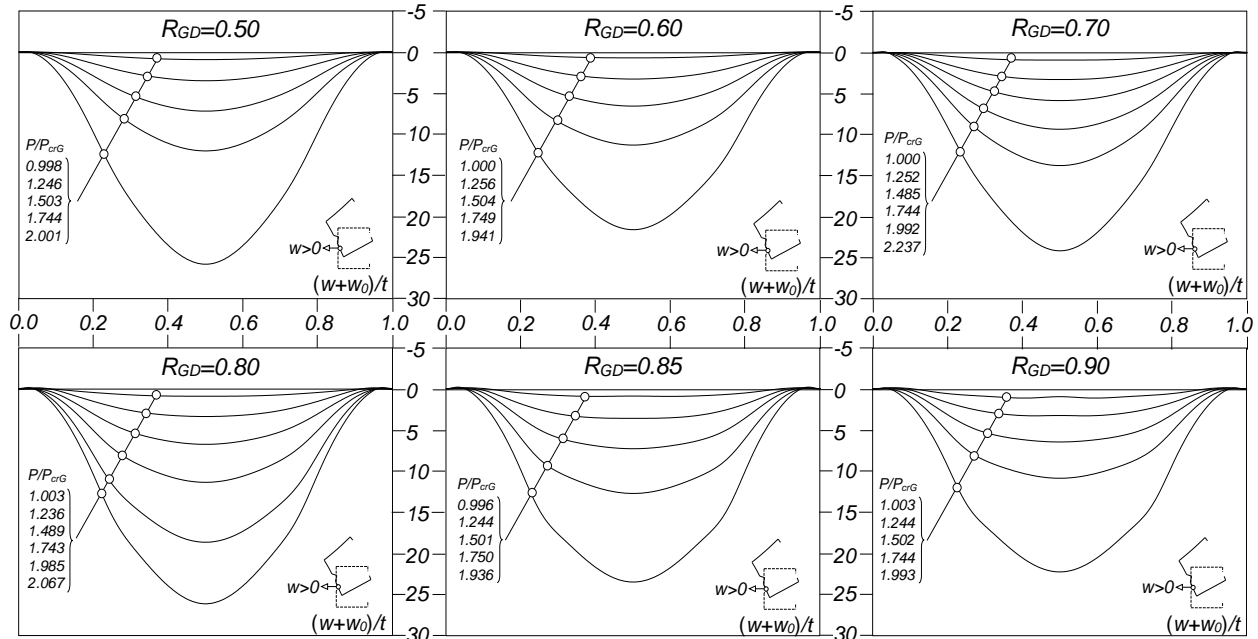


Figure 9: Mid-web transverse displacement profile evolution for the $R_{GD}=0.50, 0.60, 0.70, 0.80, 0.85, 0.90$ WSLC columns

3.2.3 Secondary-global bifurcation D-G interaction

Regardless of the cross-section shape and provided that R_y is “sufficiently high”, “secondary-global bifurcation D-G interaction” (SGI) is likely to occur, since the distortional post-critical strength reserve is much higher than its global counterpart (the opposite of what happened in the case of SDI). However, evidence of this interaction can only be clearly observed in columns containing initial geometrical imperfections akin to the critical distortional buckling mode when they are subjected to high applied load levels – indeed, only in such circumstances it is possible to observe the emergence of global deformations akin to the global buckling mode shape (regardless of its nature, which varies with the cross-section shape). Recall that, as discussed in Section 3.1, columns containing “pure” distortional imperfections exhibit a different/“unexpected” type of interaction, involving global deformation not akin to the critical global buckling mode – this type of interaction is beyond the scope of this work and, therefore, no border between distortional and SGI failures is established for such columns.

However, the inclusion of very small “global” initial geometrical imperfections makes it possible to illustrate SGI, since the “global” deformations are rapidly replaced/“swallowed” by distortional ones in the vicinity of the critical distortional buckling load. Figs. 10(a) and 11(a) show the equilibrium path of the $Z40+\lambda_D=3.5$ and $WSLC40+\lambda_D=3.5$ columns with $R_{GD}=2.0$ and containing “global” imperfections with amplitudes $L/1000$ and $L/10^6$ (values adopted in this work and used with the sole purpose of illustrating SGI, respectively). As for Figs. 10(b₁)-(d₂) and 11(b₁)-(d₂), they display several deformed configurations indicated along the equilibrium path of Figs. 10(a) and 11(a). These post-buckling results show that:

- (i) As mentioned before, the $L/1000$ columns exhibit both distortional and global deformations since that early loading stages (the latter due the initial imperfection) and, therefore, it is not possible to illustrate SGI – see the two pairs of deformed configurations depicted in Figs. 10(b₁)-(b₂) and Figs. 11(b₁)-(b₂), respectively for the Z and WSLC columns.
- (ii) SGI is clearly illustrated by the results of the $L/10^6$ columns: (ii₁) state I involves highly predominant distortional deformations, due to the column “intrinsic” post-buckling behavior (Figs. 10(c₁) and 11(c₁)) and (ii₂) global deformations only emerge and become gradually more relevant at advanced post-buckling stages – *e.g.*, see the state II deformed configurations shown in Figs. 10(c₂) and 11(c₂).

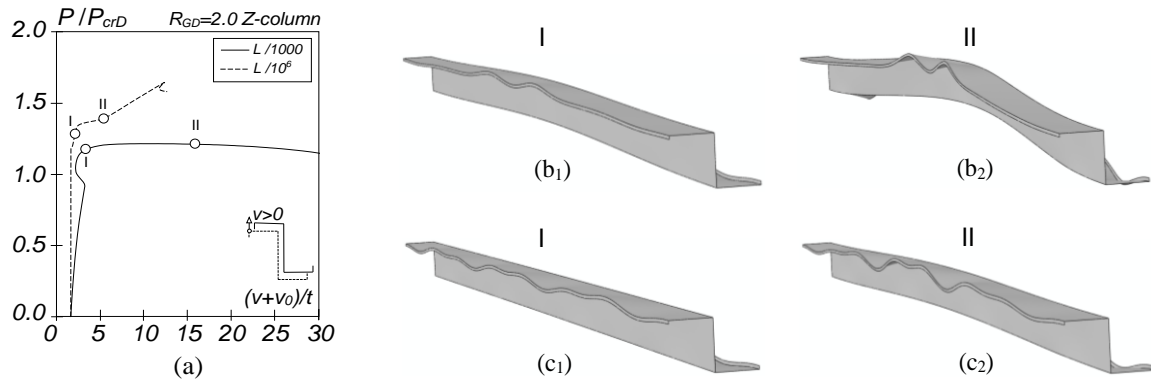


Figure 10: (a) Elastic-plastic P/P_{crD} vs. $(v+v_0)/t$ equilibrium paths of $\lambda_D=3.5$ Z40 columns with $L/1000$ and $L/10^6$ imperfections and deformed configurations of the (b) $L/1000$ and (c) $L/10^6$ columns at (1) early and (2) advanced post-buckling stages

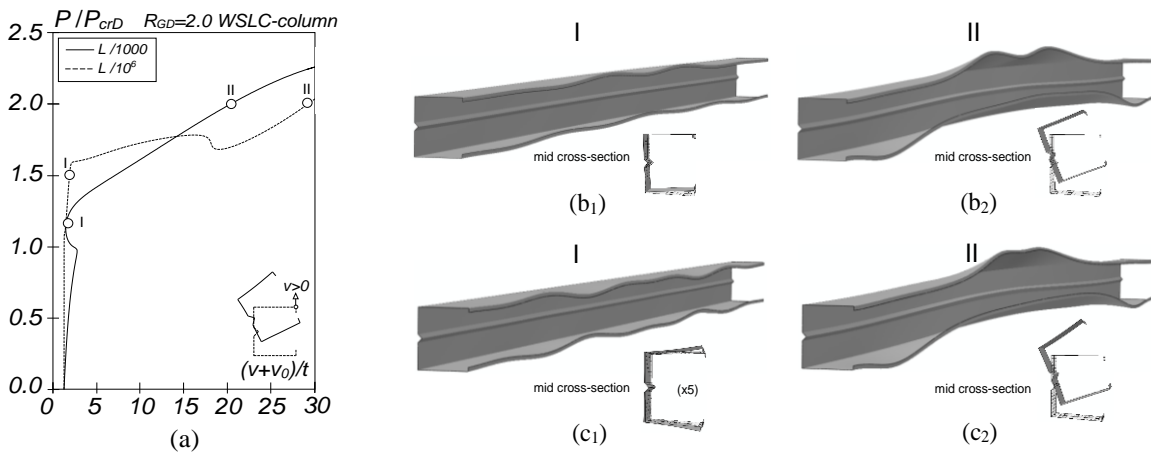


Figure 11: (a) Elastic-plastic P/P_{crD} vs. $(v+v_0)/t$ equilibrium paths of $\lambda_D=3.5$ WSLC40 columns ($L/1000$ and $L/10^6$ imperfections) and deformed configurations of the (b) $L/1000$ and (c) $L/10^6$ columns at (1) early and (2) advanced post-buckling stages

4. Direct Strength Method (DSM) Design

The Direct Strength Method (DSM), developed by Schafer & Peköz (1998b) based on an original idea from Hancock *et al.* (1994), may be viewed as an approach/procedure to establish methodologies for the design associated with a wide variety of limit states. This versatility explains the popularity of the method for the design of CFS members (and also other structural systems – *e.g.*, Schafer 2008 or Camotim *et al.* 2016b). Currently, the DSM column design (*e.g.*, AISI 2016) covers limit states associated with local, distortional, global and local-global interactive modes (for columns with or without holes/perforations) – note that the DSM global strength curve is not cast in the “Winter-type” format exhibited by their local, distortional and local-global counterparts (instead, it is a “classical” design curve taken from specifications dealing with hot-rolled steel structures). The two strength curves considered in this work are those that provide the resistance against distortional (P_{ND}) and global (P_{NG}) failures, given by the expressions

$$P_{ND} = \begin{cases} P_y & , \quad \lambda_D \leq 0.561 \\ (1 - 0.25\lambda_D^{-1.2})\lambda_D^{-1.2}P_y, & \lambda_D > 0.561 \end{cases} \quad (1)$$

$$P_{NG} = \begin{cases} 0.658\lambda_G^2 P_y, & \lambda_G \leq 1.5 \\ 0.877\lambda_G^{-2}P_y, & \lambda_G > 1.5 \end{cases} \quad (2)$$

which depend only on the elastic buckling (P_{crD} or P_{crG}) and squash (P_y) loads (the slenderness values are provided by $\lambda_D=(P_y/P_{crD})^{0.5}$ and $\lambda_G=(P_y/P_{crG})^{0.5}$). Note that AISI (2016) prescribes that the global strength curve applies to columns failing in flexural, flexural-torsional or torsional modes. One important feature of the DSM is the ability of handling explicitly interactive failures. In this regard, two design approaches can be followed (as done before for columns affected by L-D or L-G interaction): (i) the NDG approach (P_{NDG}), involving the replacement of P_y by P_{NG} in Eq. (1), as first suggested by Schafer (2002), and (ii) the NGD approach (P_{NGD}), which replaces P_y by P_{ND} in Eq. (2) – one then obtains, respectively,

$$P_{NDG} = \begin{cases} P_{NG} & , \quad \lambda_{DG} \leq 0.561 \\ (1 - 0.25\lambda_{DG}^{-1.2})\lambda_{DG}^{-1.2}P_{NG}, & \lambda_{DG} > 0.561 \end{cases} \quad (3)$$

$$P_{NGD} = \begin{cases} 0.658\lambda_{GD}^2 P_{ND}, & \lambda_{GD} \leq 1.5 \\ 0.877\lambda_{GD}^{-2}P_{ND}, & \lambda_{GD} > 1.5 \end{cases} \quad (4)$$

where $\lambda_{DG}=(P_{NG}/P_{crD})^{0.5}$ is the distortional slenderness based on the global strength and, similarly, $\lambda_{GD}=(P_{ND}/P_{crG})^{0.5}$ is the global slenderness based on the distortional strength.

4.1 Assessment of the Estimates Provided by the Global Strength Curve

Before addressing the quality of the estimates provided by the DSM global design curve for the numerical failure loads concerning columns undergoing D-G interaction, a brief study is conducted to assess how accurately does this strength curve predict load-carrying capacity of columns failing in pure global modes – a necessary first step before investigating its applicability to columns affected by D-G interaction¹⁵. Figs. 12(a)-(c) plot P_U/P_y against the “global” slenderness λ_G for two sets of Z, LC and WSLC columns

¹⁵ Note that a similar study was carried out by Landesmann & Camotim (2013) for the DSM distortional design curve – they showed that it provides accurate estimates for the load-carrying capacity of fixed-ended columns failing in pure distortional modes.

(selected in Section 2) with $\lambda_G=0.50, 0.75, 1.00, 1.25, 1.50, 1.75, 2.00, 2.50, 3.00, 3.25, 3.50$ – the DSM global strength and elastic buckling ($1/\lambda_G^2$) curves are also shown¹⁶. The observation of these results make it is possible to draw the following conclusions:

- (i) The elastic buckling curve is always above the DSM current global strength curve, which implies a minute post-critical strength. Although this is certainly true for flexural buckling, the same does not hold for flexural-torsional or torsional buckling, usually associated with a non-negligible (moderate) post-critical strength.
- (ii) Although the current specification (AISI 2016) prescribes the DSM global strength curve to predict the load-carrying capacity of columns failing in either flexural, flexural-torsional or torsional modes, the observation of Figs. 12(a)-(c) suggests that this curve is more suitable to estimate the failure loads of columns collapsing in flexural modes (Z columns – see Fig. 12(a)). On the other hand, the failure loads of the columns collapsing in flexural-torsional(-distortional) modes (LC and WSLC columns – see Figs. 12(b)-(c)) are visibly underestimated by the DSM global design curve, particularly in the moderate-to-long slenderness range ($\lambda_G > 2.0$).
- (iii) The fact that the failure loads of the two sets of columns included in each figure are predicted with different quality indicates that such quality depends on the cross-section dimensions along the whole slenderness range – this dependence is more pronounced for $\lambda_G > 1.0$, particularly in the LC and WSLC columns (failing in FTD buckling modes). Just to illustrate this assertion, note that the failure loads of the LC1 and LC2 columns with $\lambda_G=3.5$ differ by about 60%.
- (iv) Given the content of the above item, a brief study on how the column cross-section dimensions impact its post-buckling strength and failure load is presented in the next section.

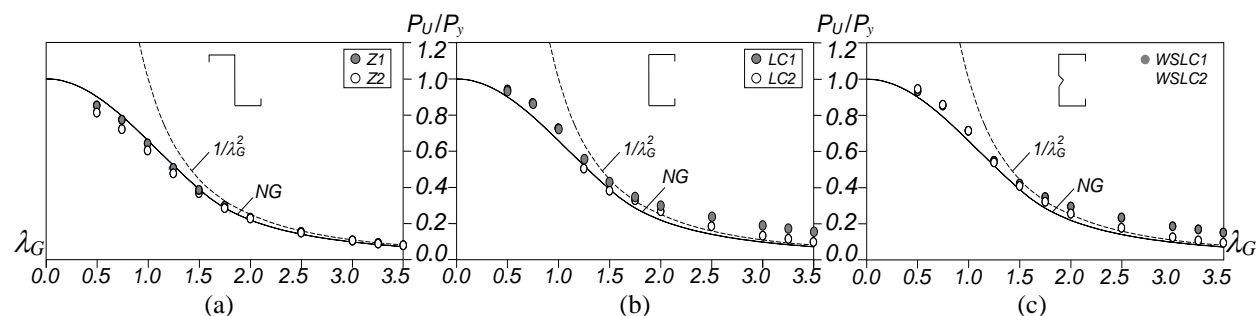


Figure 12: P_U/P_y vs. λ_G and DSM global strength curve for (a) Z, (b) LC, (c) WSLC columns failing into pure “global” modes

4.2 Influence of the Cross-Section Dimensions

In order to assess the influence of the cross-section dimensions on the ultimate strength of columns buckling and failing in FTD modes¹⁷, results making it possible to quantify the relevance of the web-to-flange (b_w/b_f) and flange-to-lip (b_f/b_l) width ratios are presented and discussed in this section. Such results concern (i) LC columns with $L=5000\text{mm}$, $t=5.0\text{mm}$, $b_f/b_l=6.0$ ($b_f=90.0\text{mm}$, $b_l=15.0\text{mm}$) and b_w/b_f equal to 1.11 ($b_w=100.0\text{mm}$), 1.33 ($b_w=120.0\text{mm}$) and 1.50 ($b_w=135.0\text{mm}$) (to assess the b_w/b_f impact), and (ii) WSLC columns with $t=5.0\text{mm}$, $b_f=10.0\text{mm}$, $b_w/b_f=1.50$ and b_f/b_l equal to 6.0 ($b_w=90.0\text{mm}$, $b_f=60.0\text{mm}$, $L=4000\text{mm}$), 8.0 ($b_w=120.0\text{mm}$, $b_f=80.0\text{mm}$, $L=7000\text{mm}$) and 10.0 ($b_w=150.0\text{mm}$, $b_f=100.0\text{mm}$,

¹⁶ Two sets of columns are considered in order to assess the influence of the cross-section dimensions on the failure load.

¹⁷ This work focuses on columns undergoing D-G interaction and investigating the influence of the cross-section dimensions on the failure load of such columns constitutes very difficult task, due to the important role played by the critical buckling load ratio R_{GD} and distortional half-wave number n_D . However, since the behavior of columns undergoing D-G interaction is mainly governed by global deformations (Martins *et al.* 2016c), it was decided to study columns buckling and failing in pure global modes instead (similar influence, hopefully).

$L=7000\text{mm}$) (to assess the b_f/b_l impact). Figs. 13(a₁)-(b₃) show elastic and elastic-plastic equilibrium paths P/P_{crG} vs. $(v+v_0)/t$ of the above six columns and their observation makes it possible to conclude that:

- (i) Ratio b_w/b_f plays an important role in the LC and WSLC column post-buckling behavior and failure load, as attested by looking at Figs. 13(a₁)-(a₃): a b_w/b_f decrease causes a significant P_U/P_{crG} increase.
- (ii) Similarly, ratio b_f/b_l also plays an important role in the WSLC (and LC) post-buckling behavior and failure load, as is clearly visible in Figs. 13(b₁)-(b₃): a b_f/b_l increase causes a drastic P_U/P_{crG} increase. Therefore, different combinations of b_w/b_f and b_f/b_l values may lead to a high variability in P_U/P_{NG} , given that P_{NG} depends only on λ_G and P_y – fortunately, the DSM global strength curve invariably underestimates the WSLC and LC column failure loads (see, for instance, Figs. 12(b)-(c)) – the amount of underestimation (safety level) depends on the combined b_w/b_f and b_f/b_l values.

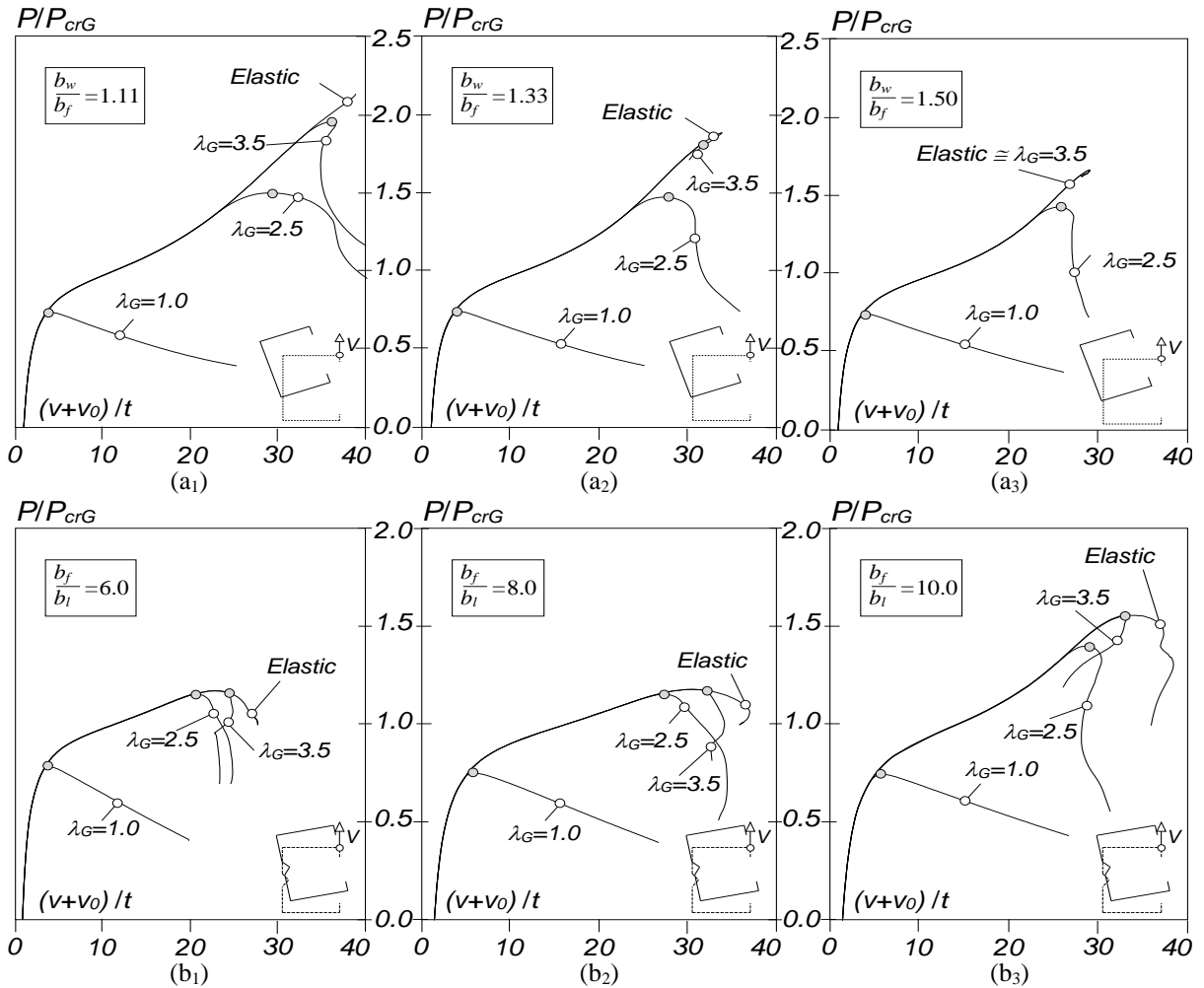


Figure 13: P/P_{crG} vs. $(v+v_0)/t$ equilibrium paths for (a) LC columns with b_w/b_f ratios equal to (a₁) 1.11, (a₂) 1.33 and (a₃) 1.50, and (b) WSLC columns with b_f/b_l ratios equal to (b₁) 6.0, (b₂) 8.0 and (b₃) 10.0

4.3 Assessment of the DSM Failure Load Estimates for Columns undergoing D-G interaction

This section addresses the DSM-based prediction of the failure loads of CFS LC, WSLC and Z columns affected by D-G interaction – although the vast majority these columns exhibit D-G interactive collapses, some of them fail in virtually pure “global” or distortional modes. Due to space limitations, the results presented and discussed concern only a representative sample of the columns identified in Section 2.

Nevertheless, they provide enough information to enable assessing the failure load prediction quality in columns exhibiting a wide variety of R_{GD} values, namely $R_{GD}=0.50-0.70-0.85-1.00-1.30-1.60-1.80-2.00$. Figs. 14(a₁)-(b) to 19(a₁)-(b₄), concerning the Z, LC and WSLC columns, respectively, display (i) P_U/P_y vs. critical slenderness (λ_D or λ_G) plots, (ii) the currently codified DSM distortional (P_{ND} vs. λ_D) or global (P_{NG} vs. λ_G) design curves, (iii) the elastic buckling curve and (iv) the two DSM-based design approaches to handle D-G interaction (P_{NDG} and P_{NGD}). To assess the overall performance of the various DSM design approaches in predicting the numerical failure load data, Figs. 20(a₁)-(d₄) plot (i) P_U/P_{NG} , P_U/P_{NDG} and P_U/P_{NGD} vs. λ_G , and (ii) P_U/P_{ND} vs. λ_D for all the Z, LC and WSLC columns considered – these figures also show the averages, standard deviations and maximum/minimum values of the above ratios. A quick observation of all these results confirms that, as it would be logical to expect after the discussions presented in the previous sections, the DSM failure load prediction quality concerning the Z and LC+WSLC columns is quite distinct – indeed, the P_U/P_y values of the two column sets are well aligned along different “Winter-type” curves. Therefore, the results concerning Z and LC + WSLC columns are addressed separately – attention is first turned to the Z columns:

- (i) The ultimate strengths of the Z columns failing in global modes ($R_{GD} \leq 0.85$ – see Section 3.2.2) are adequately predicted by the DSM global design curve, as clearly shown in Figs. 14(b₁)-(b₃) – recall that these columns do not experience SDI interaction. The P_U/P_{NG} statistical indicators given in Fig. 20(a₁) confirm this assertion: mean and standard deviation equal to 0.99 and 0.03, respectively.
- (ii) When R_{GD} increases and approaches 1.0 (Fig. 14(b₄)), the P_{NG} values gradually ceases to provide safe failure load estimates – this is because the columns are now affected to “true D-G interaction” (see Section 3.2.1). Note that the P_U/P_y values concerning these columns fall are below the DSM global design curve, even if this fact cannot be clearly observed in Fig. 14(b₄) (due to the very low P_{NG}/P_y). In order to obtain safe and accurate failure load estimates it is necessary to resort to the P_{NDG} values, which successfully account for the ultimate strength erosion due to D-G interaction.
- (iii) The DSM distortional design curve (P_{ND}) only provides adequate failure load estimates for stocky columns with $R_{DL} > 1.00$ – the number of accurate predictions grows very slowly with R_{GD} and λ_D (for instance, compare Figs. 15(a₁) and 15(a₄)), *i.e.*, when the column collapses in progressively more predominantly distortional modes (although with visible global deformations, due to the initial geometrical imperfection considered – *e.g.*, see Fig. 10(b₁)). On the other hand, the P_{ND} values overestimate the failure loads of the $R_{GD}=1.30-1.60-1.80-2.00$ slender columns (see Figs. 15(a₁)-(a₄)), thus providing clear evidence of the occurrence of D-G interaction, in this case due to “secondary global bifurcation”. Once again, the DSM-based NDG approach provides good quality predictions, as attested by looking at Fig. 20(b₁) and corresponding statistical indicators, which outperform those associated with the NGD approach – this last approach yields unsafe predictions for most slender columns ($\lambda_G \geq 2.0$ – see Fig. 20(c₁)).

Next, the observation of the results concerning the LC and WSLC columns leads to the conclusions:

- (i) Generally speaking, the DSM global strength curve is able to handle adequately all the types of failure that may occur in these columns (including some LC columns affected by L-D-G interaction). It is not necessary to resort to the NDG approach, as was done for the Z columns.
- (ii) The accuracy of the P_{NG} estimates of the ultimate strength of columns failing in “global” and D-G interactive modes (the latter due to SDI or “true D-G interaction”) depends solely on λ_G : while the failure loads of columns with $\lambda_G < 2.0$ are accurately predicted by the P_{NG} values, those of the columns with $\lambda_G > 2.0$ become increasingly underestimated (the differences can be very high – *e.g.*, they reach 250% for $\lambda_G=3.5$) – see the grey circles in Figs. 20(a₂)-(a₃). Naturally, this behavior is

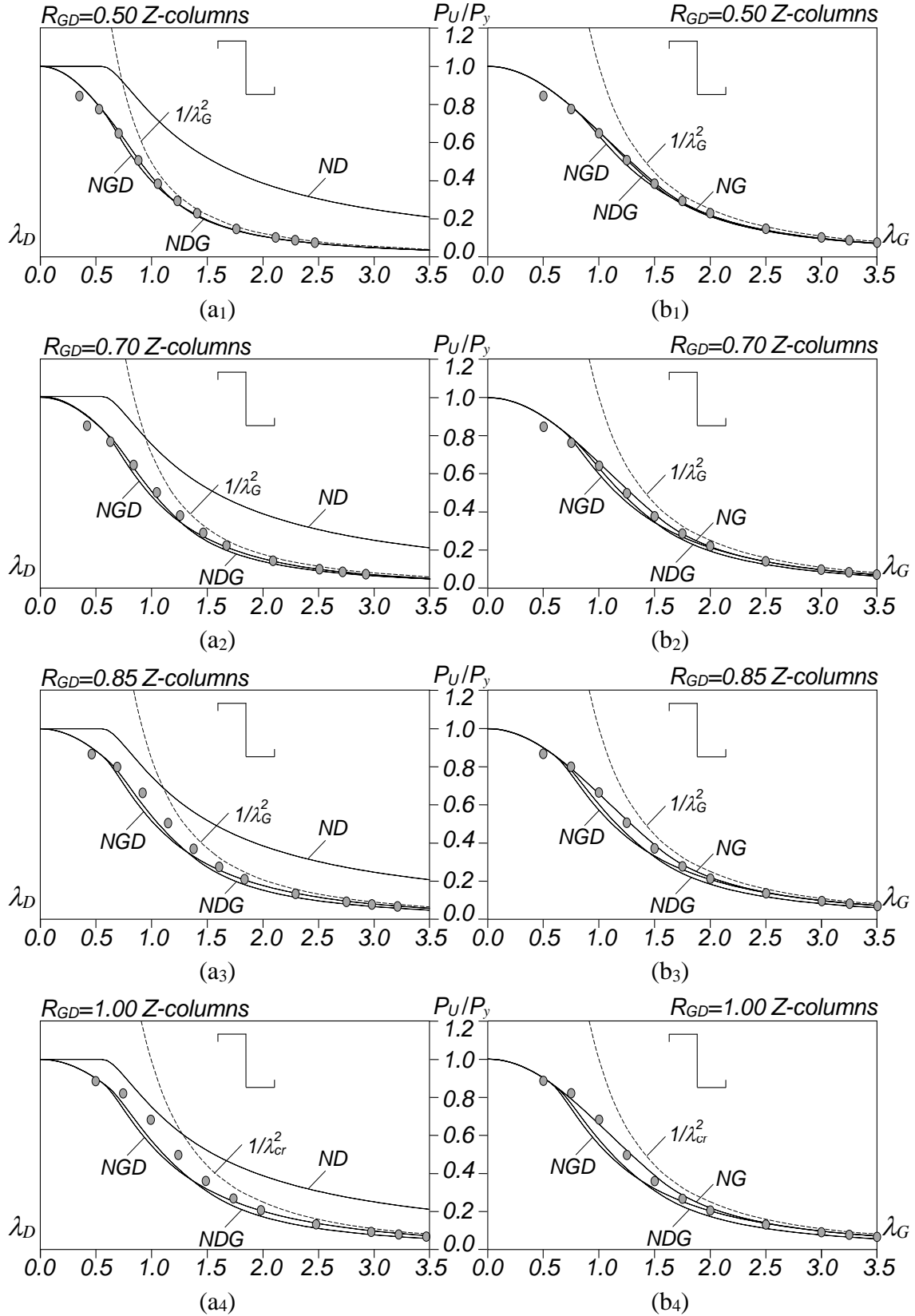


Figure 14: P_U/P_y vs. (a) λ_D or (b) λ_G plots for Z columns with (i)-(4) $R_{GD}=0.50-0.70-0.85-1.00$.

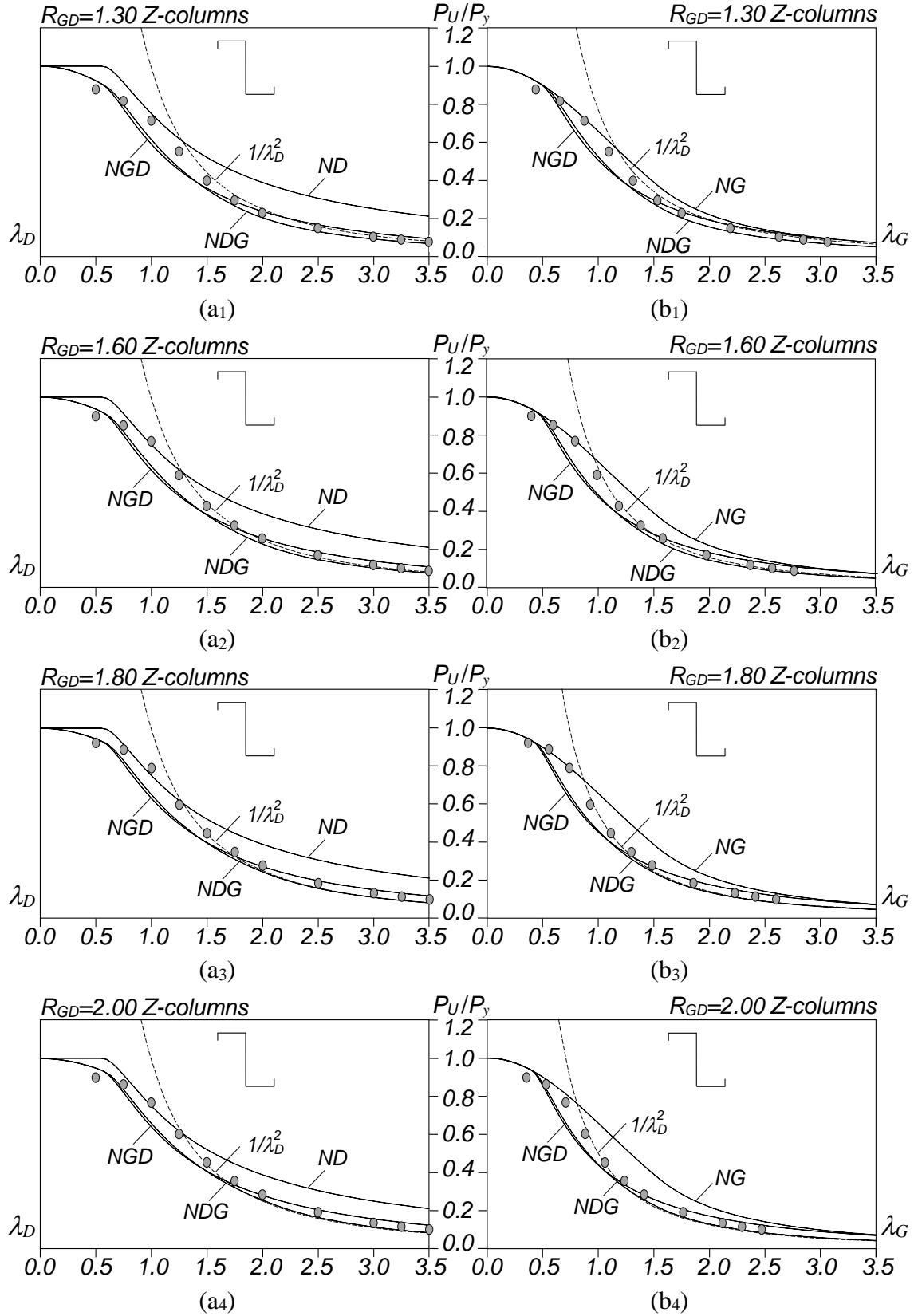


Figure 15: P_U/P_y vs. (a) λ_D or (b) λ_G plots for Z columns with (i)-(4) $R_{GD}=1.30-1.60-1.80-2.00$.

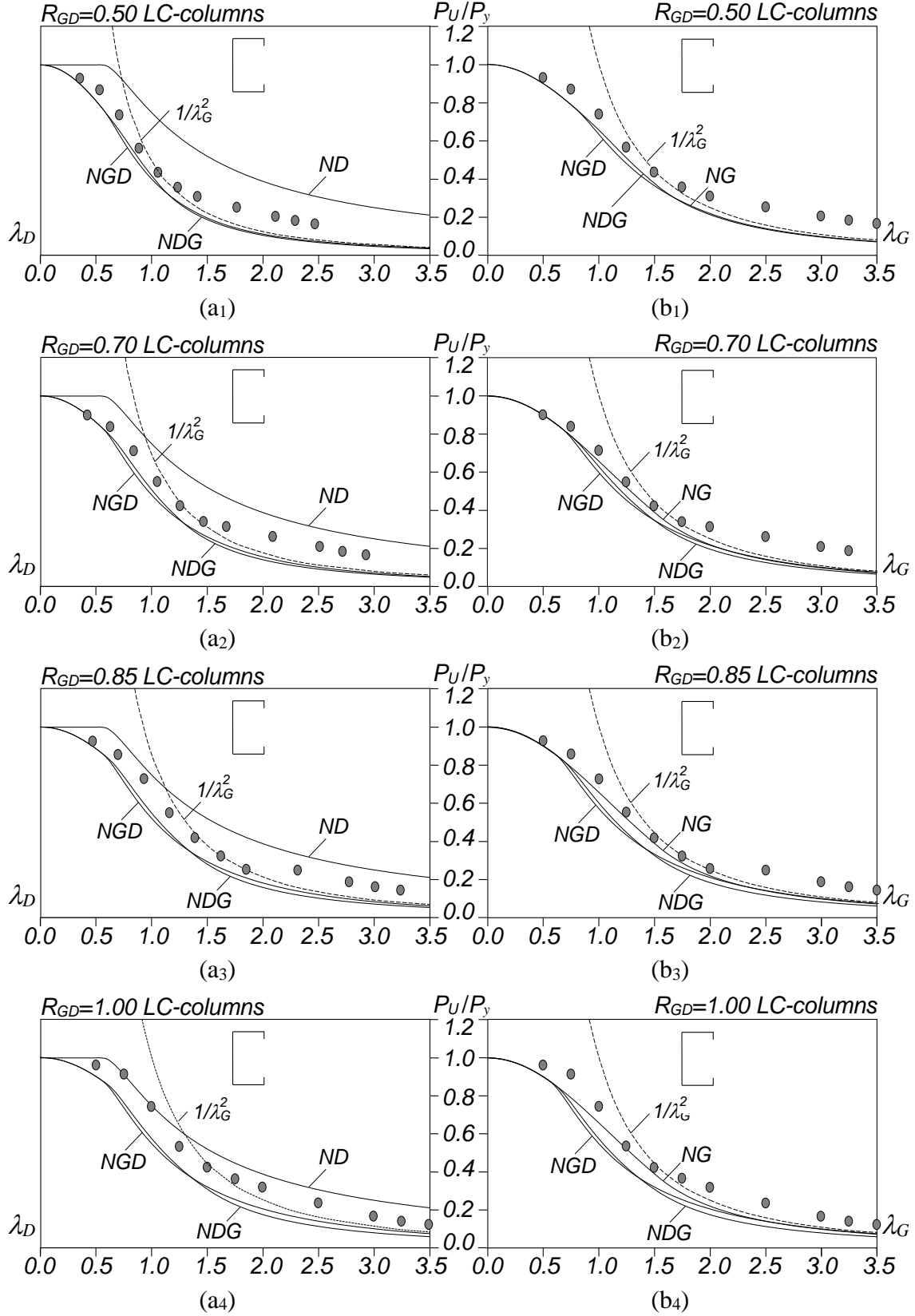


Figure 16: P_U/P_Y vs. (a) λ_D or (b) λ_G plots for LC columns with (i)-(4) $R_{GD}=0.50-0.70-0.85-1.00$.

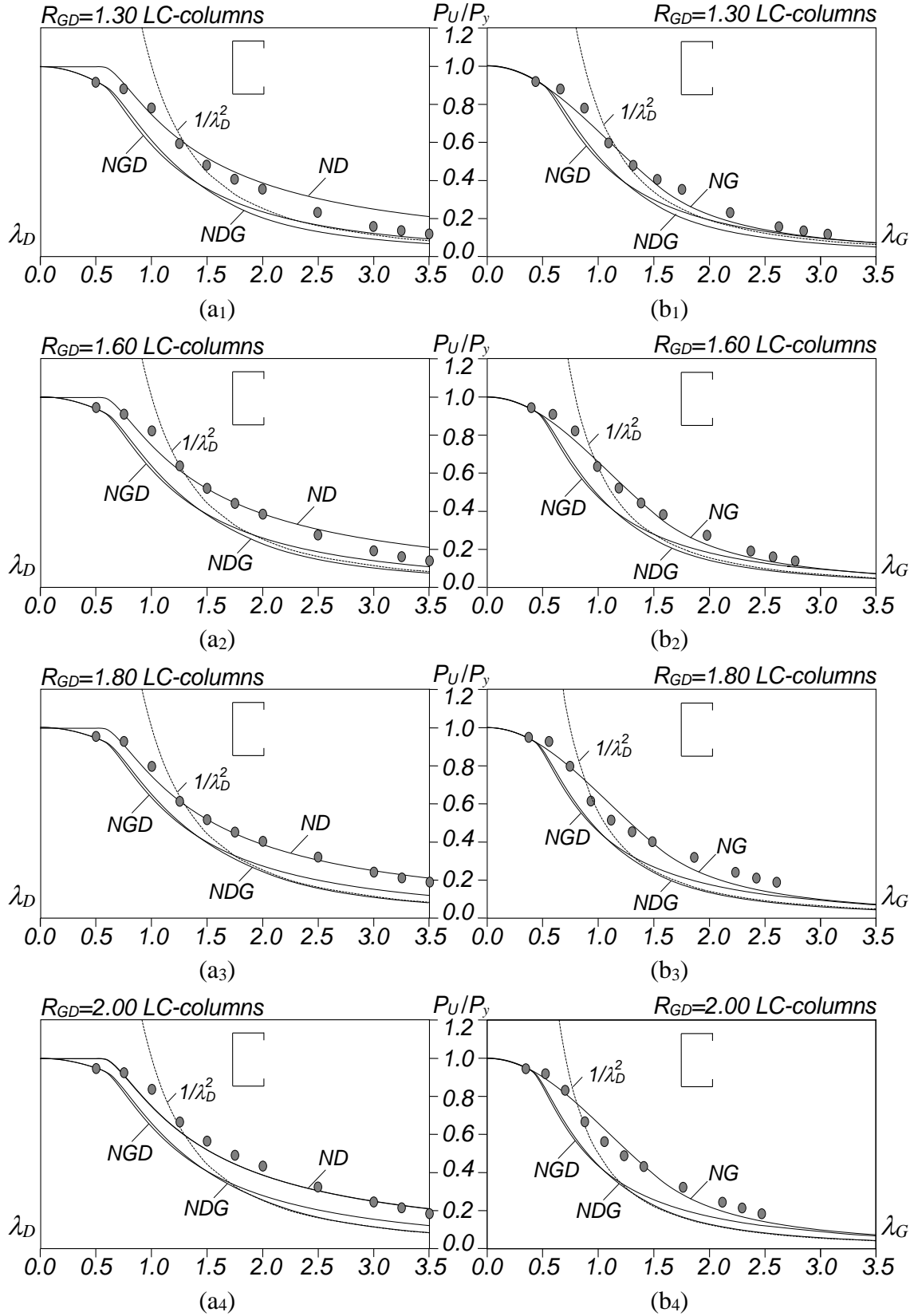


Figure 17: P_U/P_y vs. (a) λ_D or (b) λ_G plots for LC columns with (1)-(4) $R_{GD}=1.30-1.60-1.80-2.00$.

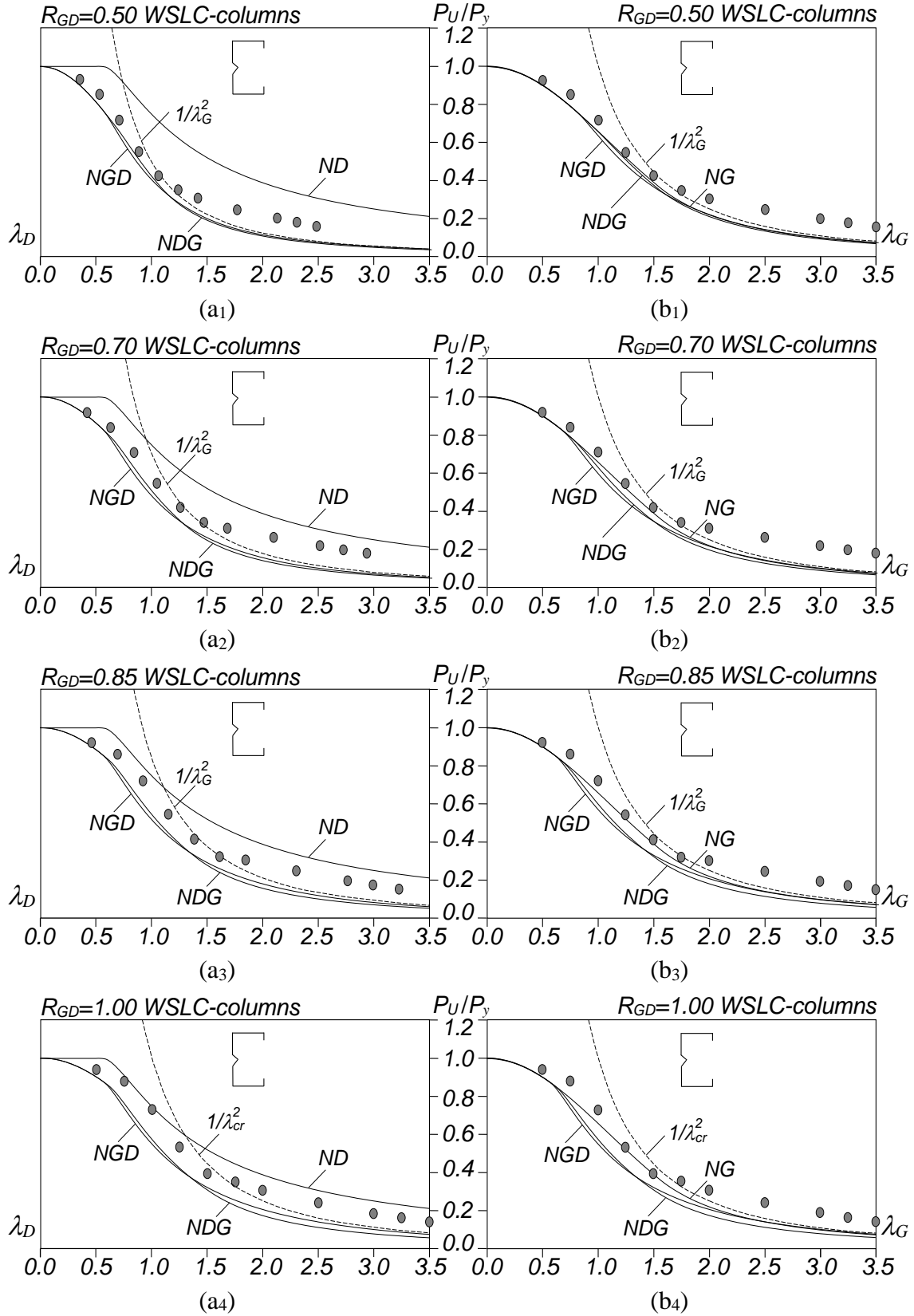


Figure 18: P_U/P_y vs. (a) λ_D or (b) λ_G plots for WSLC columns with (i)-(4) $R_{GD}=0.50-0.70-0.85-1.00$.

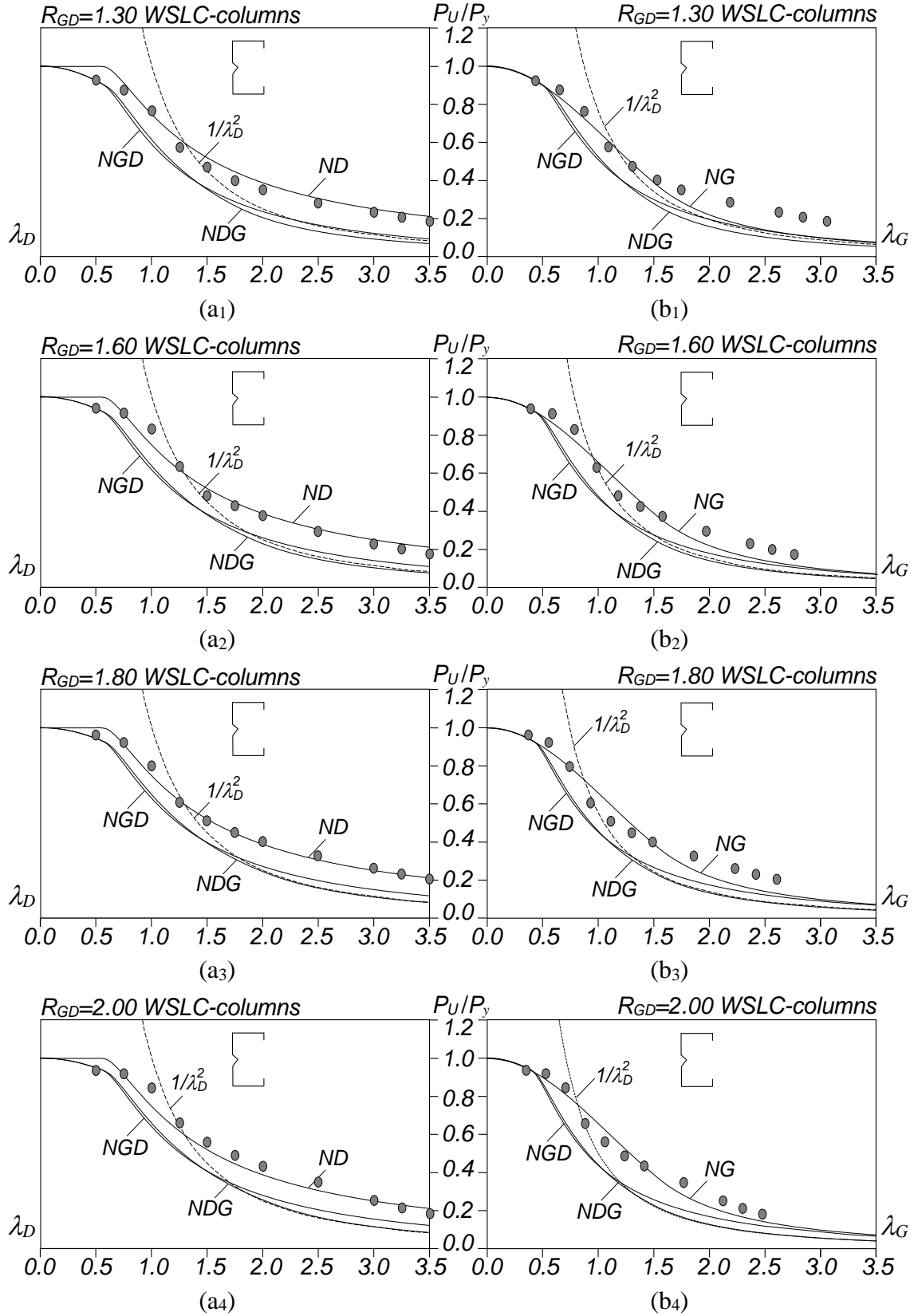


Figure 19: P_U/P_y vs. (a) λ_D or (b) λ_G plots for WSLC columns with (1)-(4) $R_{GD}=1.30-1.60-1.80-2.00$.

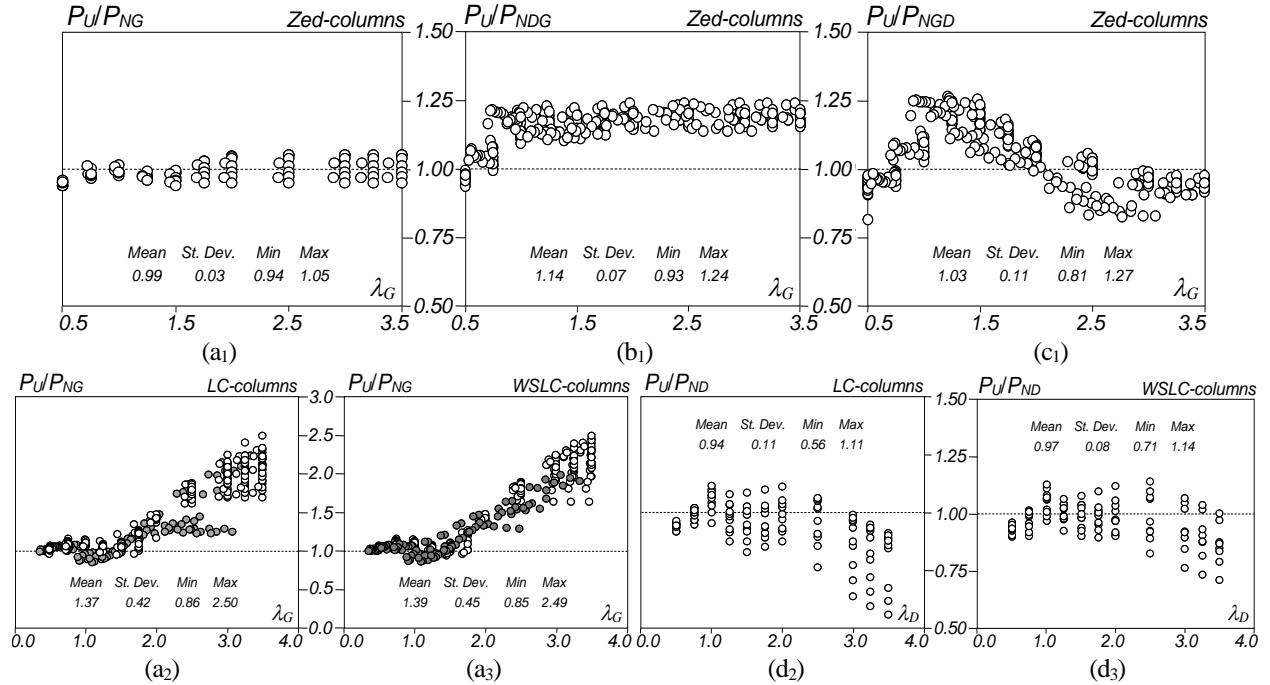


Figure 20: Plots of (a) P_U/P_{NG} , (b) P_U/P_{NDG} , (c) P_U/P_{NGD} vs. λ_G , and (d) P_U/P_{ND} vs. λ_D for (1) Z, (2) LC and (3) WSLC columns

related to the significant post-critical strength that was observed earlier and is not reflected in the P_{NG} value – see, for instance, Fig. 6(a₂)-(a₃). Indeed, even the detrimental effect stemming from the true D-G interaction may be “disguised” by this strength increase.

- (iii) A similar situation occurs for the columns failing in D-G interactive modes due to SGI ($R_{GD} > 1.0$), except for a few stocky columns, which are slightly inaccurately predicted by the P_{NG} curve (see Figs. 17(b₁)-(b₄) and 19(b₁)-(b₄) or Figs. 20(a₂)-(a₃)). These columns correspond to the transition from distortional to SGI collapses, which are logically well predicted by the P_{ND} values.
- (iv) Finally, Figs. 20(d₂)-(d₃) make it possible to assess the quality of the estimates provided by the P_{ND} values (distortional strength curve) – there exist a large number of unsafe predictions, which are particularly severe for the most slender columns (because of failure load erosion caused by the SGI).

5. Conclusions

This paper reported the available results of an ongoing SFEA investigation on the post-buckling behavior, strength and DSM design of fixed-ended cold-formed steel columns undergoing distortional-global (D-G) interaction. The columns analyzed exhibited three cross-section shapes, in order to study distinct types and natures of D-G interaction, which may involve distortional and (major-axis) flexural-torsional buckling (plain and web-stiffened lipped channel columns), or distortional and (minor-axis) flexural buckling (Z columns). Initially, a column geometry selection procedure, carried out by means of GBT buckling analyses, was employed to (i) identify fixed-ended columns geometries exhibiting a wide variety of ratios between (i₁) the distortional and global buckling loads, and (i₂) the squash and non critical buckling (distortional or global) loads, and (ii) clarify the nature of the “global” buckling loads and modes in the columns experiencing D-G interaction. Next, the elastic post-buckling behavior of the columns affected D-G interaction was thoroughly investigated and the relevance of this coupling phenomenon was assessed through elastic-plastic post-buckling analyses – the aim was to detect under which circumstances are the column ultimate strength and/or failure mode visibly affected by D-G interaction. Then, an

extensive parametric study was performed, by means of geometrically and materially non-linear ABAQUS shell finite element analyses, intended to gather failure load data concerning columns experiencing several natures/types and levels of D-G interaction. Before assessing the merits of DSM-based design approaches devised to handle this coupling phenomenon, a brief study was conducted to quantify the influence of the cross-section dimensions on the failure load of the columns under consideration. Among the various findings reported in this work, the following deserve to be highlighted:

- (i) The initial geometrical imperfection shape plays an important role in the post-buckling (elastic or elastic-plastic) behavior of columns undergoing D-G interaction, since it alters the global buckling nature. Indeed, (i₁) pure distortional initial imperfections lead to “unexpected” distortional-torsion (Z columns) or distortion-minor-axis flexure (LC and WSLC columns) interaction, while (i₂) initial imperfections with any other shape (combining the distortional and “global” buckling modes) lead to the “expected” coupling between distortional and minor-axis flexure (Z columns) or distortional, major-axis flexure, torsion and anti-symmetric distortion (LC and WSLC columns).
- (ii) The global and D-G interactive post-buckling behaviors of Z and LC+WSLC columns are very different. While the Z columns exhibit a small post-critical strength, which precludes the occurrence of “secondary-distortional bifurcation D-G interaction”, the LC and WSLC columns exhibit much larger post-critical strengths, thus making it possible for the above interaction to occur. Nevertheless, the amount of distortional deformation appearing in the failure modes is always relatively small – a similar feature was reported by Martins *et al.* 2015, in the context of columns experiencing “secondary- local bifurcation L-D interaction”).
- (iii) The emergence and development of either “true D-G interaction” or “secondary-global bifurcation D-G interaction” are possible in all columns. The former, associated with close P_{crG} and P_{crD} values, is characterized by the presence of both distortional and (predominantly) “global” deformations since the early loading stages. The latter, associated with P_{crG}/P_{crD} ratios well above 1.0, is characterized by the emergence of deformations akin to the “global” buckling mode at fairly late loading stages (provided that the yield stress is “high enough” to allow it, of course).
- (iv) The DSM global strength curve provides excellent estimates of the ultimate strength of Z columns failing in flexural modes. However, that strength curve clearly underestimates the ultimate strength of LC and WSLC columns failing in flexural-torsional modes, particularly in the moderate-to-large slenderness range (due to the non negligible post-critical strength increase mentioned in item (ii)) – the amount of underestimation depends on the combined values of the width ratios b_w/b_f and b_f/b_l .
- (v) It was found that the DSM global strength curve is able to handle adequately the three types of D-G failures occurring in LC and WSLC columns. This is because the failure load erosion stemming from the D-G interaction (which is real) is “compensated” by the safety margin of the DSM global design curve in predicting flexural-torsional failures (already mentioned in the previous items). In the Z columns, on the other hand, it is indispensable to employ the DSM-based NDG approach to capture the failure load erosion due to “true D-G interaction” and “secondary-global bifurcation D-G interaction” (“secondary-distortional bifurcation D-G interaction” is never relevant).

Finally, one last word to mention that the authors are currently working on extending this ongoing investigation to columns with other cross-section shapes, namely hat-sections and rack-sections (most likely web-stiffened, in order to preclude the occurrence of L-D-G interaction). Moreover, an attempt will be made to obtain experimental confirmation of the findings reported in this work (as mentioned in Section 1, the available experimental results concerning D-G interaction in columns are very scarce).

Acknowledgments

The first author gratefully acknowledges the financial support of FCT (*Fundação para a Ciência e a Tecnologia* – Portugal) through the doctoral scholarship SFRH/BD/87746/2012.

References

- American Iron and Steel Institute (AISI) (2016), *North American Specification (NAS) for the Design of Cold-Formed Steel Structural Members (AISI-S100-16)*, Washington DC.
- Anbarasu M, Murugapandian G (2016). Experimental study on cold-formed steel web stiffened lipped channel columns undergoing distortional-global interaction, *Materials & Structures*, **49**(4), 1433-1442.
- Bebiano R, Pina P, Silvestre N, Camotim D (2008). *GBTUL 1.0 β – Code for Buckling and Vibration Analysis of Thin-Walled Members*, DECivil/IST, Technical University of Lisbon. (available at <http://www.civil.ist.utl.pt/gbt>)
- Camotim D, Dinis PB, Martins AD, Young B (2016a). “Interactive behaviour, failure and DSM design of cold-formed steel members prone to distortional buckling”, *UBS Proceedings of 7th International Conference on Coupled Instabilities in Metal Structures (CIMS 2016 – Baltimore, 7-8/09)*, Paper KN2.
- Camotim D, Dinis PB, Martins AD (2016b). Direct Strength Method (DSM) – a general approach for the design of cold-formed steel structures, *Recent Trends in Cold-Formed Steel Construction*, C. Yu (ed.), Woodhead Publishing (Amsterdam – Series in Civil and Structural Engineering), 69-105.
- Camotim D, Dinis PB (2013). Distortional/global interaction in lipped channel columns, *Proceedings of the Institution of Civil Engineers (ICE)-Structures and Buildings*, **166**(8), 381-391.
- Crisan A, Ungureanu V, Dubina D (2012a). Behaviour of cold-formed steel perforated sections in compression – Part 1: experimental investigations, *Thin-Walled Structures*, **61**(December), 86-96.
- Crisan A, Ungureanu V, Dubina D (2012b). Behaviour of cold-formed steel perforated sections in compression – Part 2: numerical investigations and design considerations, *Thin-Walled Structures*, **61**(December), 97-105.
- Dinis PB, Camotim D (2010). Local/distortional/global buckling mode interaction in cold-formed steel rack-section columns, *Proceedings of the SSRC Annual Stability Conference (Orlando, 11-15/5)*, 481-504.
- Dinis PB, Camotim D (2011a). Post-buckling behaviour and strength of cold-formed steel lipped channel columns experiencing distortional/global interaction, *Computers & Structures*, **89**(3-4), 422-434.
- Dinis PB, Camotim D (2011b). Local/distortional/global mode interaction in simply supported cold-formed steel lipped channel columns, *International Journal of Structural Stability and Dynamics*, **11**(5), 877-902.
- Dinis PB, Camotim D (2016). Behaviour and DSM design of hat, zed and rack columns experiencing local-distortional-global interaction”, *USB Proceedings of 8th International Conference on Steel and Aluminum Structures (ICSAS 2016 – Hong Kong, 7-9/12)*, B. Young, Y. Cai (eds.), Paper 60.
- Dubina D, Ungureanu V, Crisan A (2013). Experimental evidence of erosion of critical load in interactive buckling, *Journal of Structural Engineering (ASCE)*, **139**(5), 705-716.
- Hancock GJ, Kwon YB, Bernard ES (1994). Strength design curves for thin-walled sections undergoing distortional buckling, *Journal of Constructional Steel Research*, **31**(2-3), 169-186.
- Kwon YB, Hancock GJ (1992). Tests of cold-formed channels with local and distortional buckling, *Journal of Structural Engineering (ASCE)*, **118**(7), 1786-1803.
- Landesmann A, Camotim D. (2013). On the Direct Strength Method (DSM) design of cold-formed steel columns against distortional failure, *Thin-Walled Structures*, **67**(June), 168-187.
- Martins AD, Dinis PB, Camotim D, Providência P (2015). On the relevance of local-distortional interaction effects in the behaviour and design of cold-formed steel columns, *Computers & Structures*, **160**(November), 57-89.
- Martins AD, Dinis PB, Camotim D (2016a). On the influence of local-distortional interaction in the behaviour and design of cold-formed steel web-stiffened lipped channel columns, *Thin-Walled Structures*, **101**(April), 181-204.
- Martins AD, Camotim D, Dinis PB (2016b). On the direct strength design of cold-formed steel columns failing in local-distortional interactive modes, *Proceedings of Wei-Wen Yu International Specialty Conference on Recent Research and Developments in Cold-Formed Steel Structures (Baltimore, 9-10/9)*, R. LaBoube, W.-W. Yu (eds.), 325-338.
- Martins AD, Camotim D, Gonçalves R, Dinis PB (2016c). Mechanics of distortional-global interaction in fixed-ended lipped channel columns, *USB Proceedings of 8th International Conference on Steel and Aluminum Structures (ICSAS 2016 – Hong Kong, 7-9/12)*, B. Young, Y. Cai (eds.), Paper 59.

- Rossi B, Jaspart J-P, Rasmussen KJR (2010a). Combined distortional and overall flexural-torsional buckling of cold-formed stainless steel sections: experimental investigations, *Journal of Structural Engineering* (ASCE), **136**(4), 354-360.
- Rossi B, Jaspart J-P, Rasmussen KJR (2010b). Combined distortional and overall flexural-torsional buckling of cold-formed stainless steel sections: design”, *Journal of Structural Engineering* (ASCE), **136**(4), 361-369.
- Santos ES, Batista EM, Camotim D (2012). Experimental investigation concerning lipped channel columns undergoing local-distortional-global buckling mode interaction, *Thin-Walled Structures*, **54**(May), 19-34.
- Schafer BW (2002). Local, distortional and Euler buckling in thin-walled columns, *Journal of Structural Engineering* (ASCE), **128**(3), 288-299.
- Schafer BW (2008). Review: the direct strength method of cold-formed steel member design, *Journal of Constructional Steel Research*, **64**(7-8), 766-778.
- Schafer BW, Peköz T (1998a). Computational modeling of cold-formed steel: characterizing geometric imperfections and residual stresses, *Journal of Constructional Steel Research*, **47**(3), 193-210.
- Schafer BW, Peköz T (1998b). Direct strength prediction of cold-formed steel members using numerical elastic buckling solutions, *Proceedings of 14th International Specialty Conference on Cold-Formed Steel Structures* (St. Louis, 15-16/10), W.-W. Yu, R. Laboube (eds.), 69-76.
- Silvestre N, Camotim D (2003). Non-linear generalized beam theory for cold-formed steel members, *International Journal of Structural Stability and Dynamics*, **3**(4), 461-490.
- Young B, Silvestre N, Camotim D (2013). Cold-formed steel lipped channel columns influenced by local-distortional interaction: strength and DSM design”, *Journal of Structural Engineering* (ASCE), **139**(6), 1059-1074.